



**HAL**  
open science

# Si and Ge-Based Anode Materials for Li-, Na-, and K-Ion Batteries: A Perspective from Structure to Electrochemical Mechanism

Laura Loaiza, Laure Monconduit, Vincent Seznec

► **To cite this version:**

Laura Loaiza, Laure Monconduit, Vincent Seznec. Si and Ge-Based Anode Materials for Li-, Na-, and K-Ion Batteries: A Perspective from Structure to Electrochemical Mechanism. *Small*, 2020, 16 (5), pp.1905260. 10.1002/sml.201905260 . hal-03066422

**HAL Id: hal-03066422**

**<https://hal.science/hal-03066422>**

Submitted on 15 Dec 2020

**HAL** is a multi-disciplinary open access archive for the deposit and dissemination of scientific research documents, whether they are published or not. The documents may come from teaching and research institutions in France or abroad, or from public or private research centers.

L'archive ouverte pluridisciplinaire **HAL**, est destinée au dépôt et à la diffusion de documents scientifiques de niveau recherche, publiés ou non, émanant des établissements d'enseignement et de recherche français ou étrangers, des laboratoires publics ou privés.

# Si and Ge-based anode materials for Li-, Na- and K-ion batteries: a perspective from structure to electrochemical mechanism.

*Laura C. Loaiza, Laure Monconduit, Vincent Seznec\**,

Author 1, Laura C. Loaiza

**A.** Laboratoire de Réactivité et Chimie des Solides (CNRS UMR 7314), Université de Picardie Jules Verne, 33 Rue Saint Leu, 80039 Amiens Cedex, France.

Author 2, Laure Monconduit

**B.** Institut Charles Gerhardt Montpellier, Université de Montpellier, CNRS, 34095 Montpellier, France.

**C.** Réseau sur le Stockage Electrochimique de l'Energie (RS2E), CNRS FR3459, 33 Rue Saint Leu, 80039 Amiens, Cedex, France

**D.** ALISTORE European Research Institute, Université de Picardie Jules Verne, 33 rue Saint Leu, 80039 Amiens Cedex, France

Author 3, Vincent Seznec, corresponding author

**A.** Laboratoire de Réactivité et Chimie des Solides (CNRS UMR 7314), Université de Picardie Jules Verne, 33 Rue Saint Leu, 80039 Amiens Cedex, France.

**C.** Réseau sur le Stockage Electrochimique de l'Energie (RS2E), CNRS FR3459, 33 Rue Saint Leu, 80039 Amiens, Cedex, France

**D.** ALISTORE European Research Institute, Université de Picardie Jules Verne, 33 rue Saint Leu, 80039 Amiens Cedex, France

E-mail: [vincent.seznec@u-picardie.fr](mailto:vincent.seznec@u-picardie.fr)

Keywords: anode materials, Silicon, Germanium, Battery, electrochemical mechanism

## **Abstract**

Silicon and germanium are among the most promising candidates as anodes for Li-ion batteries, meanwhile their application in Sodium- and Potassium-ion batteries is emerging. The access of their entire potential requires a comprehensive understanding of their electrochemical mechanism. This review highlights the processes taking place during the alloying reaction of Si and Ge with the alkali ions. Several associated challenges, including the volumetric expansion, particle pulverization and uncontrolled formation of SEI layer, must be surmounted and different strategies, such as nanostructures and electrode formulation, have been implemented. Additionally, a new approach based on the use of layered Si and Ge-based Zintl phases is presented. The versatility of this new whole family permits the tuning of their physical and chemical properties for specific applications. Particularly for batteries the layered structure buffers the volume expansion and exhibits an enhanced electronic conductivity allowing high power applications.

# 1 Introduction

Lithium ion batteries are the first choice of energy storage devices for portable applications.

Among all the metals Li has the smallest atomic weight and the lowest density, which

combined with a low reduction potential makes it a suitable electrode material for battery use

(**Erreur ! Source du renvoi introuvable.**)<sup>[1]</sup>The volumetric and specific capacity of sodium-ion

batteries (NIB) are much smaller than for lithium-ion batteries (LIB) due to a bigger and heavier

$\text{Na}^+$  ion and an equilibrium voltage that is 0.3 V higher than the operational potential in  $\text{Li}^+/\text{Li}$

( $E^\circ(\text{Li}^+/\text{Li})=-3.04 \text{ V}$  and  $E^\circ(\text{Na}^+/\text{Na})=-2.71 \text{ V}$ ).<sup>[2,3]</sup> In addition, the  $\text{Na}^+$  ion suffers from sluggish

diffusion and excessive volume expansion. Nevertheless NIB can be a possible contender for

LIB, given the lower Na metal cost, its higher abundance on earth's crust and precisely its

higher equilibrium potential eliminates the need of Cu current collector in the anode side,

reducing the cost of battery manufacturing.<sup>[4]</sup> The most common anode for LIB is graphite, but

it resulted to be inactive towards sodiation, opening a quest to find a suitable anode for NIB.<sup>[2]</sup>

Potassium has a similar abundance in the earth crust as Na, its equilibrium potential is 0.11 V

( $E^\circ(\text{K}^+/\text{K}) = -2.92 \text{ V}$ ) slightly higher with respect  $\text{Li}^+/\text{Li}$  and it is possible to use some of the

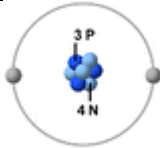
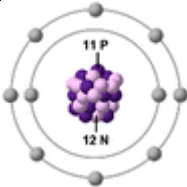
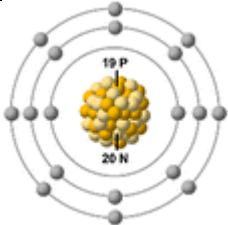
already established materials for LIB, like graphite, which is able to store K-ions.<sup>[5]</sup>

Furthermore, the  $\text{Na}^+$  and  $\text{K}^+$  ions have lower Lewis acidity compared to  $\text{Li}^+$ , meaning that their

energy for desolvation is lower. The larger alkali ions have weaker interactions with the

solvents and the anions, property that could be beneficial for high power applications.<sup>[3,6]</sup>

**Table 1.** Comparison critical parameters Li, Na and K-ion. Adapted from ref.<sup>[7]</sup>

Parameter	$\text{Li}^+$	$\text{Na}^+$	$\text{K}^+$
Ionic structure			
Ionic (Shannon) radii (Å)	0.76	1.02	1.38

Relative atomic mass	6.94	23.00	39.10
Abundance on earth crust (wt%)	0.0017	2.6	2.4
Atomic density (g cm <sup>-3</sup> )	0.534	0.968	0.89
E <sub>0</sub> versus SHE (V)	-3.04	-2.71	-2.93
Theoretical capacity (mAh g <sup>-1</sup> )	3861	1166	685
Cost of industrial grade metal (US\$/Ton)	130,000	3200	14,000

---

Concerning the anode materials used for LIB, NIB and KIB, the group 14 and 15 elements (Si, Ge, Sn, P, Sb, Bi) have been investigated (**Table 2**). Tin is electrochemically active with all three alkalis, forming Li<sub>22</sub>Sn<sub>5</sub>, Na<sub>15</sub>Sn<sub>4</sub> and KSn corresponding to a theoretical capacity of 990, 847 and 226 mAh/g, respectively. <sup>[5,8,9]</sup> The obtained experimental capacities are lower (eg. 640, 655, 180 mAh/g for Li, Na and K, respectively<sup>[6]</sup>). Phosphorus forms Li<sub>3</sub>P, Na<sub>3</sub>P and K<sub>3-x</sub>P all with a theoretical capacity of 2596 mAh/g. <sup>[4,5,7]</sup> Antimony has a theoretical capacity of 660 mAh/g for Li (Li<sub>3</sub>Sb), Na (Na<sub>3</sub>Sb) and K (K<sub>3</sub>Sb). <sup>[8]</sup> Silicon displays a capacity of 4200 mAh/g for Li<sub>22</sub>Si<sub>5</sub> and 3579 mAh/g for Li<sub>15</sub>Si<sub>4</sub>. <sup>[10,11]</sup> Theoretical studies have predicted the reaction of Si with Na and K with theoretical capacities of 954 mAh/g for NaSi <sup>[12]</sup> and 995 mAh/g for KSi<sup>[5]</sup>. In both cases the reaction suffers from poor kinetics and experimentally the c-Si has been considered to be inactive or at least partially inactive towards Na and K, however a-Si appears to be a potential candidate. <sup>[5,13-17]</sup> Germanium, reacts with Li to form Li<sub>22</sub>Ge<sub>5</sub> and Li<sub>15</sub>Ge<sub>4</sub> with capacities of 1623<sup>[18]</sup> and 1384 mAh/g <sup>[19]</sup>, respectively. The sodiation presents a theoretical capacity of 369 mAh/g, experimental values around 350 mAh/g corresponding to the formation of NaGe have been found. <sup>[9]</sup> The potassium insertion in Ge has a theoretical capacity of 369 mAh/g. <sup>[20]</sup> All the elements in this group suffer volume variations upon alloying reaction, in general with increasing alkali content and cation size the highest is the volume expansion. <sup>[3,5,6,8]</sup> This represents a critical issue to address before these materials can achieve practical commercial applications. Indeed the subsequent volume changes produces particle cracking, that upon repetitive cycling will lead to particles pulverization and detachment from the current

collector. In addition the crack formation expose new electrode surface to the electrolyte, promoting a continuous and uncontrolled formation of Solid electrolyte interphase (SEI) on the particles and a high coulombic unefficiency. Several strategies have been proposed in the literature to address these challenges, including the electrode architecturing and nanostructuring, electrolyte formulation, use of composite electrodes and prelithiation processes, choice of binder, among others.

**Table 2.** Theoretical capacities of lithiation, sodiation and potassiation of group 14 and 15 elements and their approximated volume expansion after alloying reaction.

Material	Alkali	Stoichiometry final product	Theoretical Capacity (mAh/g)	Approximated Volume change (%)
<b>Sn</b> <sup>[5]</sup>	Li	Li <sub>22</sub> Sn <sub>5</sub>	990	676
	Na	Na <sub>15</sub> Sn <sub>4</sub>	847	420
	K	KSn	226	180
<b>P</b> <sup>[5]</sup>	Li	Li <sub>3</sub> P	2596	200
	Na	Na <sub>3</sub> P	2596	390
	K	K <sub>3-x</sub> P	≤2596	Not known
		KP	843	190
<b>Sb</b> <sup>[5]</sup>	Li	Li <sub>3</sub> Sb	660	147
	Na	Na <sub>3</sub> Sb	660	390
	K	K <sub>3</sub> Sb	660	407
<b>Si</b> <sup>[10–12,21,22]</sup>	Li	Li <sub>22</sub> Si <sub>5</sub>	4200	400
		Li <sub>15</sub> Si <sub>4</sub>	3579	270
	Na	NaSi	954	114
	K	KSi	995	334
<b>Ge</b> <sup>[9,18–20,23]</sup>	Li	Li <sub>22</sub> Ge <sub>5</sub>	1623	370
		Li <sub>15</sub> Ge <sub>4</sub>	1384	250
	Na	NaGe	369	225
	K	KGe	369	Not known

The challenges introduced by the use of Si- and Ge-based anodes for LIB, NIB and KIB require the understanding of the whole picture of the electrochemical processes taking place in the battery, which are too often neglected when designing new electrodes. In this review we begin by a revision of the electrochemical mechanism of Si and Ge in order to understand the

different phenomena related with the cycling. Following a short revision of the different strategies used for addressing capacity fading in Si and Ge electrodes is presented before introducing a new family of compounds, the so-called Zintl phases, which have potential applications as anode for LIB, NIB and KIB. In this last section the particularities and versatility of this family of compounds will be discussed, featuring their potential advantages over other conventional battery materials

## 2 Electrochemical mechanism insight

Both silicon and germanium are known to undergo an alloying reaction with Li, Na and K (**Equation 1**) that in most cases delivers higher theoretical capacities compared to the conventional carbon-based anodes. (

Figure 1). Nonetheless, it is accompanied by a huge volume expansion and particle pulverization that is detrimental for the electrode.

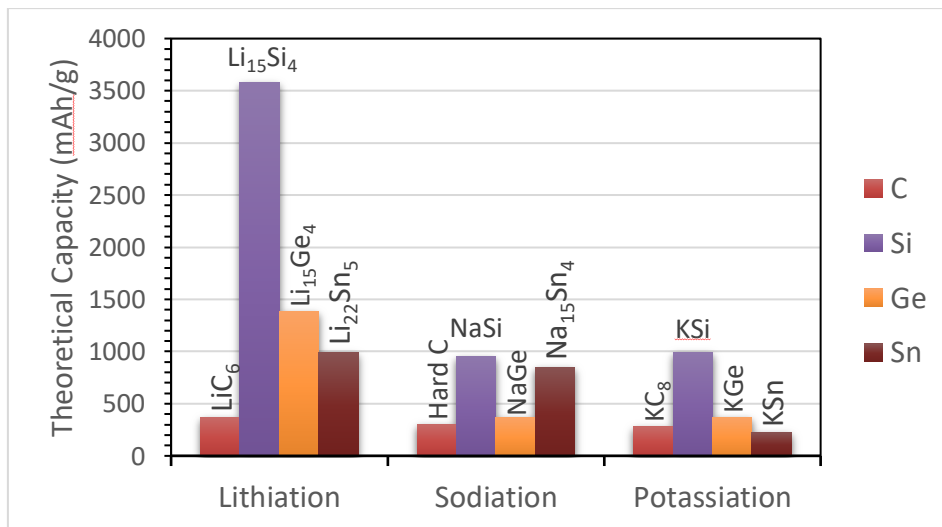
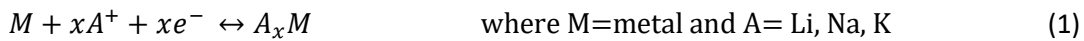


**Figure 1.** Theoretical capacities of lithiation, sodiation and potassiation of C, Si, Ge, Sn. Adapted from ref. [5,24].

Before advancing in details into the electrochemical mechanism it is important to review the profile of the galvanostatic cycling of Si and Ge since the information they provide is crucial for the understanding of all the phenomena taking place during cycling.

## 2.1 Galvanostatic cycling of Si and Ge

The electrochemical behavior of silicon has been widely studied in the literature. The galvanostatic cycling of c-Si (**Figure 2a**), is characterized by a rapid decrease in the potential until reaching a plateau between 120 and 80 mV, then there is a change in slope close to the end of the discharge where the potential rapidly decreases.<sup>[25]</sup> During charge the processes take place at higher voltages, the potential increases rapidly until 0.4 V followed by a plateau, after which the slope increases upwardly suggesting a one-phase region. For the second discharge at least two different plateaus are observed.<sup>[25]</sup> These processes can be evidenced in the derivative curve (**Figure 2b**) by three reduction peaks and a very sharp oxidation one.

For nano-silicon (**Figure 2-c**), during the first discharge, the galvanostatic profile is the same as in bulk silicon. The main difference appears upon charge, where instead of a rapid increase in the voltage to 0.4 V followed by a plateau there is a gradual increase in the voltage. In the second discharge two plateaus appear in nano Si at 0.25 V and 0.10 V, indicating a different reaction compared to the first discharge.<sup>[26]</sup> Regarding the lithiation of amorphous silicon, initially it occurs at a higher potential compared to c-Si, but this potential decreases as the lithiation proceeds. In order to keep the lithiation in the amorphous region the cutoff voltage must be set before the crystallization of c-Li<sub>15</sub>Si<sub>4</sub>.<sup>[27]</sup>

For the case of germanium (**Figure 3**), the electrochemical response presents four main processes during the lithiation. From 1.0 to 0.7 V the continuous drop in potential is attributed to partial reduction of the electrolyte leading to the formation of the solid electrolyte interphase (SEI) at the surface of the electrode.<sup>[28-30]</sup> From  $\approx 380$ -250 mV and  $\approx 250$ -150 mV, two pseudo-plateaus indicate the coexistence of two phases, and are followed by a drop of the potential (after ca. 200 mV), corresponding to a one-phase region. Upon delithiation, the slope increases abruptly until approximately 350 mV, followed by the presence of two pseudo-plateaus at 420-450 mV. The second lithiation is slightly different, the first pseudo-plateau (at



410 mV) presents a steeper slope, whereas the second (at 250 mV) is more marked. Both processes, however, occur at higher potentials, suggesting the electrochemical path followed during the second discharge is possibly different. All the processes in the galvanostatic curves are well defined in the derivative curves, except for the intensities of the peak at 590 mV during charge and the broadening of the peak at 380 mV during the second discharge indicative of a change in the nature of the Ge network compared to the pristine sample.

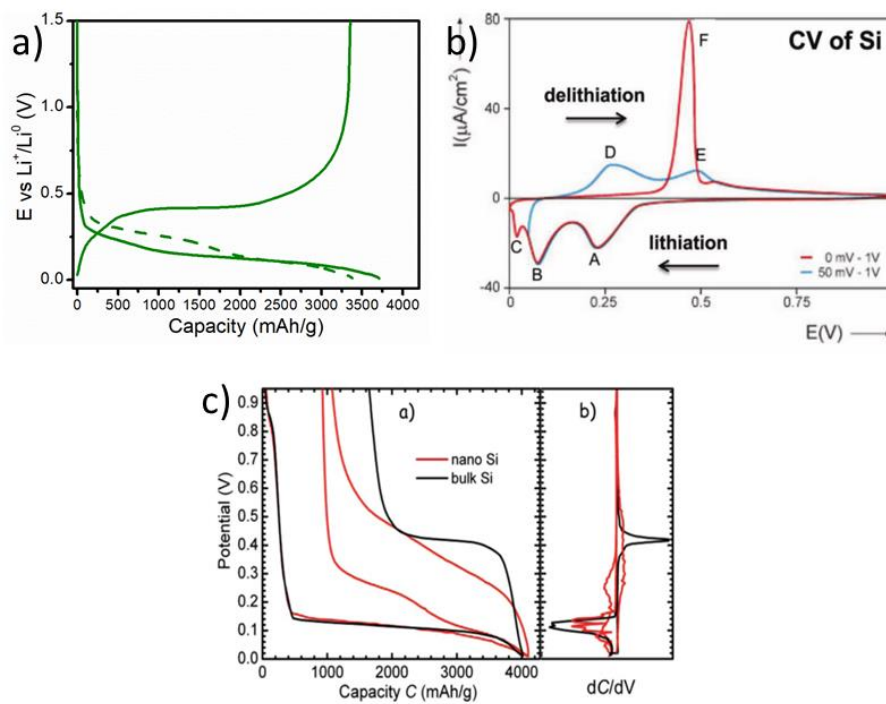


**Figure 2.** **a)** Galvanostatic curve of Si cycled vs Li, **b)** Cyclic voltammetry of Si vs Li with 0 V and 50 mV cut-off voltage, <sup>[31]</sup>**c)** Galvanostatic curve of nano- and bulk-Si vs Li and their respective derivative curves. <sup>[26]</sup>

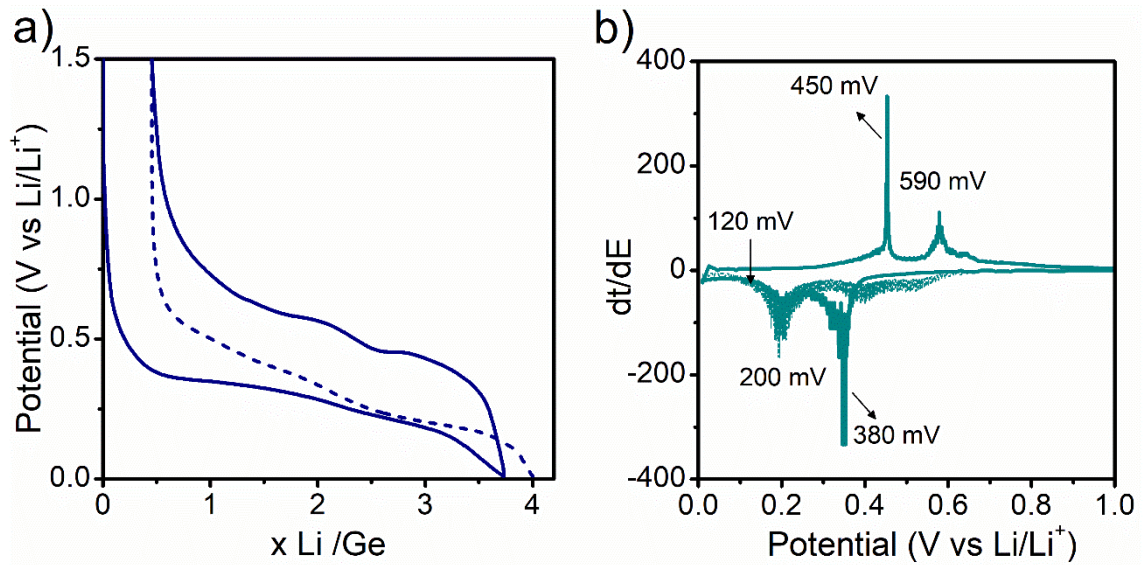


**Figure 3.** Galvanostatic discharge-charge curves of the Ge electrode at **a)** C/5 and **b)** its corresponding derivative curve.

According to the literature the plateau during the first discharge is associated with the amorphization of the c-Si (Ge) into a-Li<sub>x</sub>Si (a-LiG<sub>x</sub>e) intermediates, with the crystallization of c-Li<sub>15</sub>Si<sub>4</sub> (Li<sub>15</sub>Ge<sub>4</sub>) at the end of discharge. These both phases are very similar, crystallize in the same space group I-43d and their lattice parameters differ in as little as 0.9%.<sup>[32]</sup> The delithiation proceeds with the amorphization of this crystalline Li<sub>15</sub>Si<sub>4</sub> (Li<sub>15</sub>Ge<sub>4</sub>) phase and at the end of the process an amorphous Si (Ge) network is obtained. This last one can be affected by a series of factors like structure or residues of c-Si (c-Ge) in the electrode. The second and subsequent lithiation/delithiation of a-Si (a-Ge) are characterized by gently sloping profile indicating that the process occurs in the amorphous phase, then the energy differences between all the formed phases are smaller, the lithiation will occur preferentially on the previously lithiated regions. It is worth to note, that the formation of c-Li<sub>15</sub>Si<sub>4</sub> has an impact over the profile of the galvanostatic and derivative curves, this is, if the cutoff voltage reaches values below 100 mV, the derivative curve displays a reduction peak at low voltages marked as C in **Figure 2-b**, while the delithiation is characterized by a plateau at 0.45 V and a sharp oxidation peak (F) in the derivative curve, the magnitude and the sharpness of the peak are measure of the presence of Li<sub>15</sub>Si<sub>4</sub> at full lithiation. On the contrary, if the cell voltage is limited

to 100 mV (avoiding the process C), there is a change in the galvanostatic profile for the first charge where no clear plateau can be evidenced, characteristic of processes in the amorphous phase, and the delithiation will be characterized by two broad peaks (D and E) (**Figure 2-b**).

<sup>[25,33]</sup> The nature of these processes is not yet well understood and could be highly dependent on other factors such as dopants or structure of the Si. <sup>[31,33,34]</sup> The suppression of the formation of  $\text{Li}_{15}\text{Si}_4$  has been observed at high C/rates due to a kinetic limitation to achieve full lithiation, translated into a decrease in the capacity <sup>[35]</sup> and for films of thicknesses lower than 500 nm. <sup>[36]</sup> Nevertheless, this last one is subject of debate, according to Obrovac <sup>[37]</sup> during the first 20 cycles of lithiation/delithiation of a Si thin film the profile of the derivative curve is similar to a-Si, but after continuous cycling the sharp peak near 0.42 V typical of the formation of  $\text{Li}_{15}\text{Si}_4$  appears. Indeed, the formation of c- $\text{Li}_{15}\text{Si}_4$  is believed to be the responsible for the delamination of the Si films after certain cycles. <sup>[37]</sup>

Despite the similarities between Si and Ge their lithiation phase formation sequences, kinetics and mechanical responses are different. For instance, for Silicon the lithiation of the crystalline phase happens in an anisotropic way and is governed by the movement a two-phase boundary between the inner crystalline Si core and the outer amorphous  $\text{Li}_x\text{Si}$  alloys. Note that this is only applicable for the first cycle, after which the silicon remains amorphous. <sup>[38]</sup> The lithiation of a-Si is isotropic and leads as well to the formation of a- $\text{Li}_x\text{Si}$  intermediates. <sup>[31,32]</sup> At the end of discharge, the spontaneous crystallization of  $\text{Li}_{15}\text{Si}_4$  is not common in other alloy anodes, in which crystalline phases are attained via a two-phase reaction that implies nucleation and growth processes. For instance as the x value in a- $\text{Li}_x\text{Si}$  approaches 3.75, the electronic structure of  $\text{Li}_{3.75}\text{Si}$  becomes very similar to the  $\text{Li}_{15}\text{Si}_4$ , the phase transformation is possibly driven by the similarities of the electronic structures between the amorphous and the crystalline phases at high Li contents. This process only takes place electrochemically and no composition fluctuations are observed during the crystallization. The formation energies of  $\text{Li}_{15}\text{Si}_4$  must be then lower than the amorphous counterparts and other crystalline phases with

similar composition like  $\text{Li}_{12}\text{Si}_7$  and  $\text{Li}_{13}\text{Si}_4$ . Thus the lithiation mechanism of Si does not follow the thermodynamically stable phases in the phase diagram. <sup>[24,31,36]</sup>

The lithiation of germanium is isotropic; this difference compared to Si lies in the properties of the crystallographic planes of unlithiated Si (Ge) crystals that adjoin the amorphous product. This is, the orientation dependence of interfacial mobility at the sharp boundary of the two phases (pristine crystal and amorphous lithiated intermediates) is expected to govern the lithiation anisotropy in Si, rather than the long-range transport. While Si has a preferential lithiation the (110) planes, Ge does not experience such phenomena and lithiates evenly in all the directions without the formation of cracks during lithiation. These factors influence greatly the final electrochemical performance and in general an isotropic expansion is favoured in order to extend the lifetime of the battery. <sup>[31,39]</sup> In the case of germanium compared to silicon the Li diffusion is about 400 times faster <sup>[40]</sup> and the electronic conductivity is two orders of magnitude higher. <sup>[41]</sup> In parallel with Si, the lithiation happens from the surface of the particles to the core, with the cracks nucleating in the particle edges and propagating inwards. <sup>[39,42]</sup> During its lithiation the Ge-Ge bonds gradually break to form  $\text{a-Li}_{2.26}\text{Ge}$  and later  $\text{a-Li}_{3.5}\text{Ge}$  (like in the crystalline  $\text{Li}_7\text{Ge}_2$ ). Both phases are constituted of Ge dumbbells and isolated Ge atoms, since these motifs are present in several  $\text{Li}_x\text{Ge}$  phases with similar structures and formation energies the transformation might not be linear and several other intermediates could be involved. As the lithiation proceeds, the number of isolated Ge atoms increases and the crystallization of  $\text{c-Li}_{15}\text{Ge}_4$  is energetically favoured. <sup>[18,43]</sup> Indeed, for Ge the nature of the formed phases depends on particles size and morphology and cycling conditions like C-rate or electrode formulation, these factors affect the kinetics of phase formation. <sup>[18,44,45]</sup>

## 2.2 Alloying mechanism

### 2.2.1 Lithiation

The understanding of the behavior of Si in a battery is crucial, but the phase diagram based on thermal processes does not necessarily represent the processes taking place in a battery. A typical phase diagram includes LiSi, Li<sub>12</sub>Si<sub>7</sub>, Li<sub>13</sub>Si<sub>4</sub> and Li<sub>22</sub>Si<sub>5</sub>, all of them with less formation energy for the crystalline phases than for the amorphous one. However during lithiation no crystalline phases are formed despite their lower Gibbs free energy. The Li<sub>x</sub>Si products are always amorphous with composition 0 < x < 3.75, at x = 3.75 the crystallization of a phase takes place through a spontaneous process without long-distance atomic diffusion. For a long time this crystalline phase was presumed to be Li<sub>22</sub>Si<sub>5</sub>/Li<sub>21</sub>Si<sub>5</sub><sup>[46,47]</sup> but in 2004 Obrovac<sup>[48]</sup> established it as Li<sub>15</sub>Si<sub>4</sub> corresponding to the most lithiated phase formed electrochemically at room temperature while Li<sub>22</sub>Si<sub>5</sub>/Li<sub>21</sub>Si<sub>5</sub> can only be obtained for very slow rate cycling at T° > 100°C. <sup>[49,50]</sup> The Li<sub>15</sub>Si<sub>4</sub> has lower formation energy than other alloys with the same Li content and it is metastable, decomposing rapidly into other lithiated compounds such as Li<sub>13</sub>Si<sub>4</sub>, Li<sub>7</sub>Si<sub>3</sub> or other weakly crystallized phases. <sup>[31,51]</sup>

The *in situ* and *ex situ* XRD analysis (**Figure 4**) of the electrochemical lithiation mechanism of Si, indicates a gradual decrease in the diffraction peaks of c-Si upon lithiation, corresponding to the amorphization of the crystalline network. Following the system shows no diffraction peaks indicating the presence of amorphous phases, until 100 mV where a phase corresponding to Li<sub>15</sub>Si<sub>4</sub> starts to crystallize, which below 50 mV is transformed into a non-stoichiometric phase c-Li<sub>15+δ</sub>Si<sub>4</sub>.<sup>[34]</sup> All these processes are in line with the previous description of the plateau and peaks in the galvanostatic and derivative curves respectively for the first discharge. During charge, the diffraction peaks associated with c-Li<sub>15</sub>Si<sub>4</sub> gradually disappear, in agreement with the plateau and peak at around 0.4 V in the galvanostatic and derivative curve, respectively, indicators of the amorphization of c-Li<sub>15</sub>Si<sub>4</sub>. At the end of charge an amorphous pattern is recorded. <sup>[33]</sup> The presence of amorphous silicon, influences the potentials at which the processes take place during the second discharge with the formation of a-Li<sub>x</sub>Si intermediates at

higher potential values compared to the first discharge, while the crystallization of c-Li<sub>15</sub>Si<sub>4</sub> happens at a slightly lower potential. [52] [25]

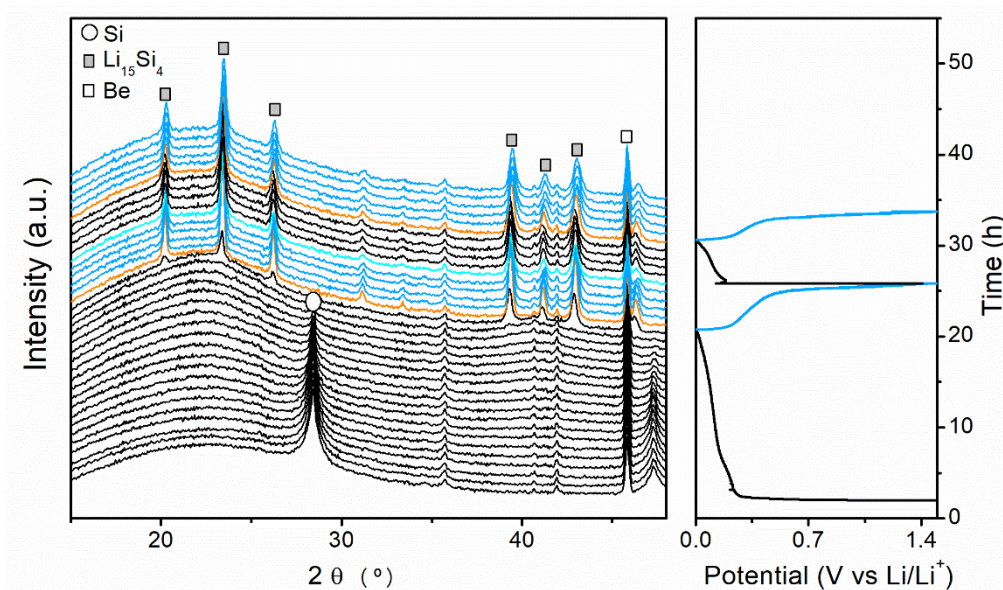


**Figure 4.** In situ XRD for a self-supported Si electrode cycled vs Li at a rate of C/5.

Given the amorphous nature of the different lithiated intermediates in the Li-Si system, alternative studies such as NMR, XAS, Raman, among others, must be implemented in order to study the short-range order interactions and relate them with the electrochemistry phenomena. For instance Grey *et al* [41,53–55] have devoted great part of their studies to the identification of these intermediates, indeed the lithiation happened to be more complicated than previously thought and dependent on several factors. By studying the <sup>7</sup>Li NMR, it is possible to identify different lithiated intermediates. The lithiation starts by the Si surface, the presence of Li in the Si framework eventually results in the breaking of the Si-Si bonds, with the loss of all the long range ordering in c-Si and the formation of small Si clusters. Given the large associated energy to break the crystalline Si network, once the lithiation has started and the small clusters are formed (stars, rings and dumbbells), it is kinetically easier to continue breaking these clusters than the original Si framework. Both processes compete and prevent the system to reach equilibrium. Due to the inhomogeneity of the processes, no single type of

cluster is present at this stage, hindering the crystallization of any phase as it will require bond breakage and rearrangement involving high activation energies. The breakage of the small clusters continues until the formation of mainly isolated Si ions, from which the c-Li<sub>15</sub>Si<sub>4</sub> nucleates. The preference in the nucleation of c-Li<sub>15</sub>Si<sub>4</sub> over Li<sub>22</sub>Si<sub>5</sub> (a phase composed also of isolated Si ions), lies in the ability of the first one to accommodate defects such as the dumbbells that are presumed to remain at this stage.<sup>[34]</sup> Additionally the atomic arrangements of a-Li<sub>3.75</sub>Si and c-Li<sub>15</sub>Si<sub>4</sub> are very similar, favoring the crystallization of this last one and no other phase.<sup>[36]</sup>

These phenomena originate characteristic Li environments that are related with the degree of lithiation (**Figure 5**). This is, as the Li/Si ratio increases the chemical shift moves to lower frequencies and the shielding around the Li ions increases: i) signals between 16-22 ppm are attributed to small Si clusters like in Li<sub>12</sub>Si<sub>7</sub> (planar Si<sub>5</sub> rings and Si<sub>4</sub> stars), ii) signals between 12-14 ppm are attributed to Si dumbbells like in Li<sub>7</sub>Si<sub>3</sub>, iii) signals between 8-10 ppm describe lithium ions interacting with both dumbbells and isolated Si<sup>4+</sup> ions like in Li<sub>13</sub>Si<sub>4</sub>, iv) signals between 3-6 ppm describe Li interacting exclusively with isolated Si ions like in Li<sub>15</sub>Si<sub>4</sub>, v) signals between -1 to 3 ppm are attributed to Li species in the SEI layer. Finally signals with negative shift are attributed to the formation of the overlithiated phase Li<sub>15+δ</sub>Si<sub>4</sub>.<sup>[34,56-58]</sup> This last one is only observed for the *in situ* experiments, and the negative shift suggest a more shielded environment. This resonance grows at the expense of the peaks with positive shifting, its intensity is enhanced by holding the voltages at 0 V but it rapidly disappears if the cell is relaxed, however no change in the macrostructure is detected at this stage. Li<sub>15</sub>Si<sub>4</sub> is an electron deficient phase with high degree of defects, hence it can accommodate extra Li to form c-Li<sub>15+δ</sub>Si<sub>4</sub>, since for the system it is more favored to further lithiate c-Li<sub>15</sub>Si<sub>4</sub> than to convert the residual a-Li<sub>x</sub>Si into c-Li<sub>15</sub>Si<sub>4</sub> originating the negative shift in the NMR experiment. These results indicate that the lithiation process is inhomogeneous and is related to the different cycling conditions, defects, particle size, etc.<sup>[34,56-58]</sup> For instance an electrochemically

formed  $c\text{-Li}_{15+\delta}\text{Si}_4$  phase from a pristine Si electrode presents a different  $^7\text{Li}$  NMR shift compared to the one obtained from mechanically synthesized  $c\text{-Li}_{15}\text{Si}_4$  (discharged to 0V). [34,57] Finally the formation of  $c\text{-Li}_{15}\text{Si}_4$  is incomplete, in some cases there are residual unbroken Si-Si pairs that limit the maximum of Li atoms that can be bonded to Si, explaining the inability of the system to go towards higher x values,  $x=4.2$  or  $4.4$  like in  $\text{Li}_{21}\text{Si}_5$  and  $\text{Li}_{22}\text{Si}_5$ . [59]

On the other hand, if the cutoff voltage is set to 85 mV, at this stage there are more clusters than isolated Si ions. Hence, upon delithiation, these clusters serve as nucleation sites for the reconstruction of the amorphous network by the addition of isolated ions and/or the fusion of several small clusters. This is translated in a decrease in the signal of the 18-16 ppm peak after 300 mV. This peak shifts to lower frequencies close to 10 ppm at around 450 mV, indicating a depletion of small clusters due to a preferential delithiation while the isolated Si ions are still present in the system (like in  $\text{Li}_{13}\text{Si}_4$ ). Beyond this point the 10 ppm resonance disappears and a new one appears at 3 ppm nearly at the end of charge. [34]

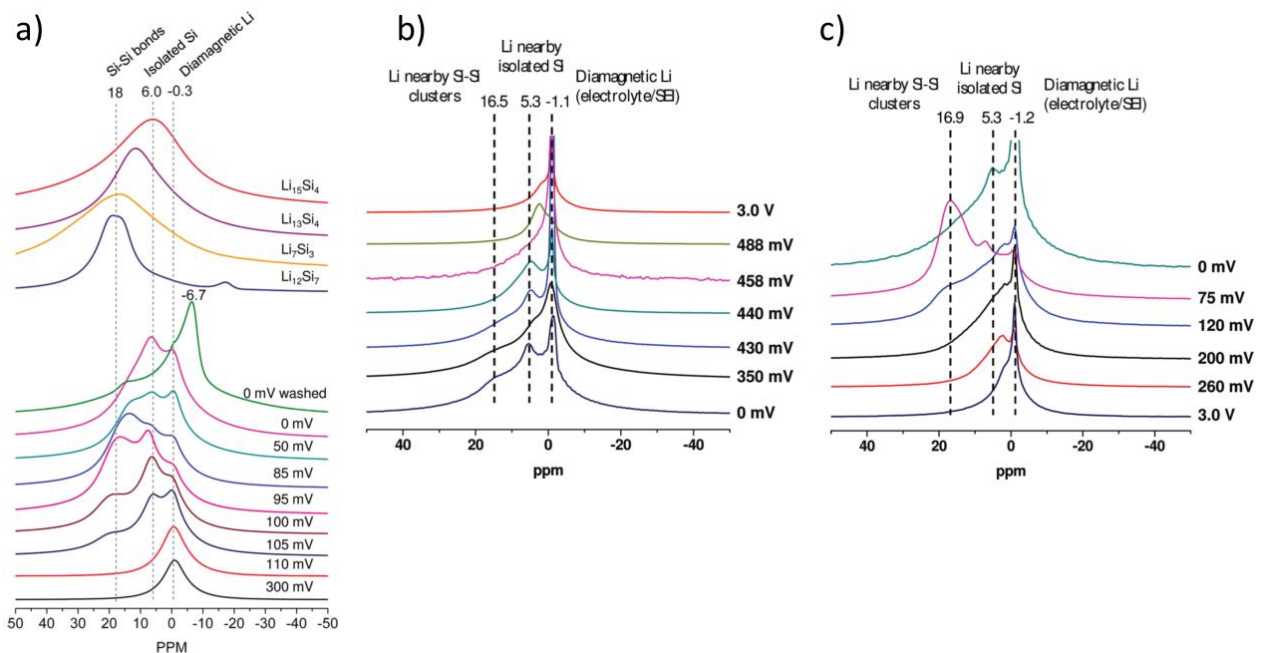




**Figure 5.** Ex Situ  $^7\text{Li}$  NMR MAS of batteries stopped at a selected potential during a) first discharge, b) first charge and c) second discharge. <sup>[34]</sup>

For Ge, few information is focused on the basic lithiation mechanism. <sup>[18,30,45,60–62]</sup> Some studies demonstrate that the Ge particles size and morphology have a strong impact on the lithiation mechanism and stabilized phases. <sup>[18,30,43,45,60–64]</sup> Indeed, in analogy with the lithiation of silicon, the XRD findings show amorphization of c-Ge upon lithiation, followed by the formation of amorphous lithiated intermediates and the crystallization of c-Li<sub>15</sub>Ge<sub>4</sub> at the end of discharge while the charge happens almost completely in the amorphous phase. The results are, however, difficult to rationalize; even if it seems clear that crystalline Li<sub>15</sub>Ge<sub>4</sub> and Li<sub>15+δ</sub>Ge<sub>4</sub> are the end-products under electrochemical conditions, there is still no consensus on the different intermediated phases. Moreover, the presence of such intermediate phases depends strongly on the current density, revealing the importance of kinetics in the electrochemical mechanism.

**Table 3.** Literature review of the chemical species formed during lithiation of germanium electrodes.

Author (ref.)	Type of electrode	C/Rate	Proposed species during lithiation	Identification Technique
Yoon <i>et al.</i> <sup>[63]</sup>	Micrometric-sized c-Ge and Carbon-coated composite prepared by mechanical ball milling and pyrolysis.	100 mA/g	c-Li <sub>9</sub> Ge <sub>4</sub> c-Li <sub>7</sub> Ge <sub>2</sub> c-Li <sub>15</sub> Ge <sub>4</sub> c-Li <sub>22</sub> Ge <sub>5</sub>	Ex situ XRD
Baggetto <i>et al.</i> <sup>[30,60]</sup>	Evaporated/sputtered a-Ge thin film (50 nm thickness)	C/20	a-LiGe a-Li <sub>7</sub> Ge <sub>2</sub> c-Li <sub>15</sub> Ge <sub>4</sub>	In situ XRD In situ XAS
Graetz <i>et al.</i> <sup>[28]</sup>	Evaporated/ballistically deposited a-Ge thin film	C/4	c-LiGe c-Li <sub>7</sub> Ge <sub>2</sub> c-Li <sub>15</sub> Ge <sub>4</sub> c-Li <sub>11</sub> Ge <sub>6</sub> c-Li <sub>9</sub> Ge <sub>4</sub> c-Li <sub>22</sub> Ge <sub>5</sub> a-Li <sub>x</sub> Ge c-Ge upon delithiation	Ex situ XRD
Lim <i>et al.</i> <sup>[61]</sup>	Micrometric-sized c-Ge	C/15	a-Ge a-Li <sub>9</sub> Ge <sub>4</sub>	Operando XRD and XAS

			a-LiGe a-Li <sub>7</sub> Ge <sub>2</sub> a-Li <sub>x</sub> Ge c-Li <sub>15</sub> Ge <sub>4</sub>	
<b>Lim et al</b> [45,62]	Micrometric-sized c-Ge	$>C/5$ $C/5 < C < C/10$  $C/20$	a-Li <sub>x</sub> Ge a-Ge a-Li <sub>x</sub> Ge a-Li <sub>9</sub> Ge <sub>4</sub> c-Li <sub>15</sub> Ge <sub>4</sub>  a-Li <sub>x</sub> Ge c-Li <sub>15</sub> Ge <sub>4</sub>	Operando XRD and XAS
<b>Jung et al</b> [18]	Micrometric-sized c-Ge	C/50	c-Li <sub>7</sub> Ge <sub>3</sub> a-Li <sub>7</sub> Ge <sub>2</sub> a-Li <sub>13</sub> Ge <sub>5</sub> c-Li <sub>15</sub> Ge <sub>4</sub> c-Li <sub>15+6</sub> Ge <sub>4</sub>	Ex situ XRD In situ/Ex situ Solid state NMR Pair Distribution Function
<b>Loaiza et al</b> [44]	Micrometric-size c-Ge	$C/5-C/8$  $C/14$	a-LiGe a-Li <sub>7</sub> Ge <sub>3</sub> c-Li <sub>15</sub> Ge <sub>4</sub>  a-Li <sub>x</sub> Ge c-Li <sub>17</sub> Ge <sub>4</sub>	Operando XRD, XAS and Raman Spectroscopy.
<b>Tang et al</b> [43]	Ge Nanorods embedded in multiwall carbon nanotubes	C/5	a-Li <sub>2,26</sub> Ge a-Li <sub>3,5</sub> Ge c-Li <sub>15</sub> Ge <sub>4</sub> c-Li <sub>15+6</sub> Ge <sub>4</sub>	In situ XRD In situ Solid State NMR
<b>Morris et al</b> [64]	---	---	LiGe Li <sub>7</sub> Ge <sub>3</sub> Li <sub>13</sub> Ge <sub>5</sub> Li <sub>8</sub> Ge <sub>3</sub> Li <sub>15</sub> Ge <sub>4</sub> Li <sub>17</sub> Ge <sub>4</sub>	Density Functional Theory calculations

In analogy with Si, the information obtained by XRD is very limited and other characterization techniques are implemented. **Table 3** shows some of the different intermediates and the respective characterization techniques used to identify. It is worth to note that Graetz *et al.* [28] have identified some of the lithiated intermediates by *ex-situ* XRD, this point is particularly surprising given the fact that later reports identify most of the intermediates to be amorphous phases, hence, the presence of crystalline phases in this study might be related with the sample treatment before the XRD analysis, which given the metastable nature of the involved phases could induce to their crystallization. The XAS technique has been implemented commonly for the identification of the intermediates, and phases such as a-LiGe, a-Li<sub>7</sub>Ge<sub>2</sub>, a-Li<sub>7</sub>Ge<sub>3</sub> and a-Li<sub>9</sub>Ge<sub>4</sub> have been identified. These phases

present very similar properties and their interpretation from the results could vary depending on the used method. It is concluded as well that one or more of the previous phases coexist at the same potential, thus the lithiation process is highly inhomogeneous. [44,60,61,65] The solid state NMR is another powerful technique to identify the different lithiated intermediates which in analogy to the findings for silicon have a characteristic signal at different frequencies. In this sense, signals between 20-25 ppm are attributed to phases with Ge dumbbells like in  $\text{Li}_7\text{Ge}_3$  and  $\text{Li}_9\text{Ge}_4$ , with the formation of  $\text{Li}_7\text{Ge}_3$  being more energetically favored. Signals between 12-14 ppm are attributed lithium ions interacting with both dumbbells and isolated  $\text{Ge}^{4-}$  ions like in  $\text{Li}_7\text{Ge}_2$  and  $\text{Li}_{13}\text{Ge}_4$ . Signals between 0-10 ppm describe Li interacting exclusively with isolated Ge atoms like in  $\text{Li}_{15}\text{Ge}_4$ , while the ones between -24 to -21 ppm featured a process of overlithiation of the  $\text{Li}_{15}\text{Ge}_4$  into  $\text{Li}_{15+6}\text{Ge}_4$ . This process of overlithiation is identified merely by means of NMR spectroscopy, where it is possible to observe the difference of the chemical shift of the phase due to a new Li environment that is more shielded. Other characterization techniques did not show any difference in the results at this voltage. Indeed the  $\text{Li}_{15}\text{Ge}_4$  is an electron deficient phase and can accommodate extra charges without any change in the crystal structure, this is a purely electrochemical driven reaction that terminates once the cell is allowed to rest at OCV. [41,43]

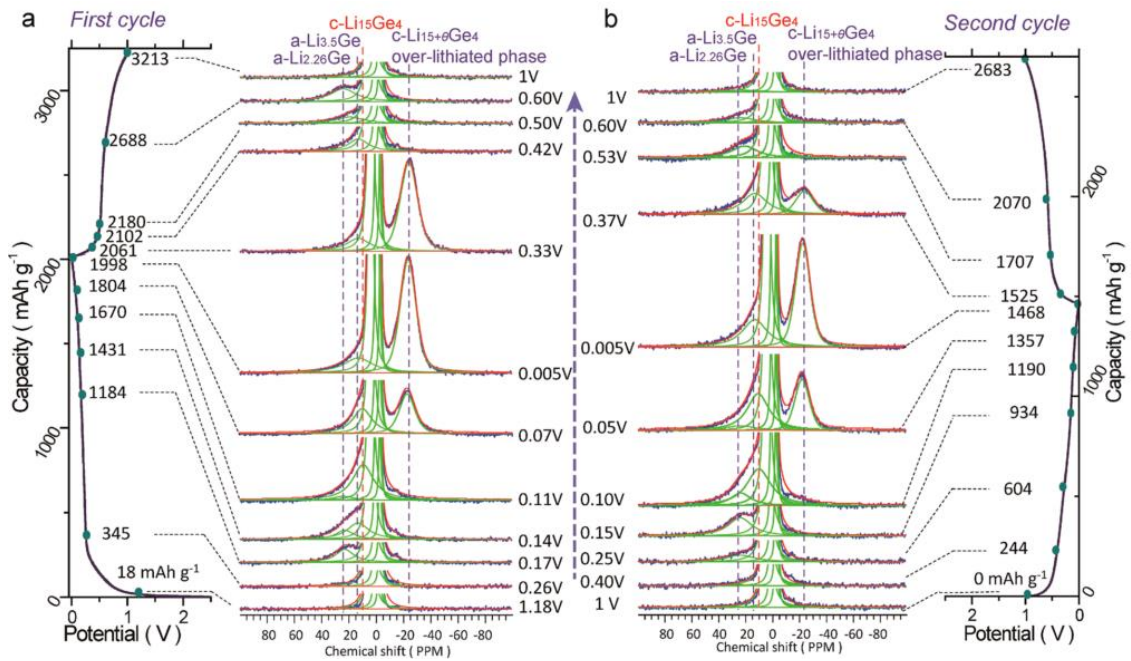


**Figure 6.** Stacked in situ  ${}^7\text{Li}$  NMR of a Ge-carbon nanotube composite obtained during the **a)** first and **b)** second discharge/charge cycles. <sup>[43]</sup>

### 2.2.2 Sodiation.

The sodiation of silicon has been less investigated, whether crystalline Si is electrochemically inactive or at least partially is subject of debate, one can find reports supporting both statements. This reaction is considered to be impeded by the poor Na kinetics and the positive binding energy during the sodiation of c-Si. <sup>[12,13,66]</sup> Some authors have reported the sodiation of nano-sized c-Si, which after the first sodiation is transformed in a-Si, the following cycles take place in the amorphous domain. Micron-sized c-Si does not experience a sodiation process. <sup>[14,15]</sup> On the contrary, the sodiation of amorphous Si is possible. According to the Na-Si phase diagram the most sodiated phase has a composition 1:1, leading to a theoretical capacity of 954 mAh/g. <sup>[12]</sup> Recently a theoretical report showed that the maximum Na storage in Si is 0.76 Na, corresponding to a theoretical capacity of 725 mAh/g. <sup>[67]</sup> Experimentally it is not clear how many atoms of Na can be stored in Si, neither the achievable capacities or which dimensional scale or form (nano, micron, amorphous, crystalline) is required. <sup>[17]</sup> Reports in the literature have showed the feasibility of sodiation of a-Si, yet with severe transport limitations that can be partially improved by electrodes nanodesigning. <sup>[12,13]</sup>

In analogy with Si, the insertion of sodium in c-Ge is almost negligible. The major obstacle lies in the high diffusion barrier for Na in Ge lattice, due to its larger size the activation energy for migration between the interstitial sites in the lattice is higher (1.5eV for Na compared to 0.51eV for Li).<sup>[68]</sup> Still, c-Ge can be amorphised after the first discharge/charge cycle while the sodiation continues in the amorphous phase.<sup>[68]</sup> Amorphous Ge is active towards sodiation,<sup>[20,69]</sup> the phase diagram indicates NaGe as the most sodiated phase, but recent reports have shown the insertion of more than one sodium in the Ge lattice, corresponding to Na<sub>1.6</sub>Ge.<sup>[68,70]</sup> In addition, GeO<sub>x</sub> has shown some activity vs Na, with the formation of Na<sub>2</sub>O that serves as a buffer to accommodate the volume changes during cycling.<sup>[71,72]</sup>

### 2.2.3 Potassiation

The knowledge regarding alloying compounds with potassium is limited. It has been theoretically predicted that Si undergoes this reaction to form KSi with 955 mAh/g. This process is expected to happen through a series of alloys, like K<sub>12</sub>Si<sub>17</sub>, K<sub>7</sub>Si<sub>46</sub>, K<sub>8</sub>Si<sub>46</sub> and KSi. Crystalline silicon is believed to be inactive towards potassiation.<sup>[5]</sup> Yet, theoretical predictions indicate that amorphous Si can store up to 1.1 K-ion leading to a theoretical capacity of 1049 mAh/g, the K-ion can diffuse rapidly in the a-Si network, due to the weak electrostatic K-Si attraction and the formation of isolated Si<sub>n</sub> clusters during the potassiation.<sup>[22]</sup> Experimentally, few work has been performed, Sultana *et al*<sup>[5]</sup> reported the electrochemical inactivity of Si with K, whereas Komaba *et al*<sup>[6]</sup> presented in a preliminary study of the potassiation of a-Si with a capacity of 510 mAh/g. In the case of germanium, the crystalline phase shows no activity while the amorphous counterpart is expected to form KGe with a theoretical capacity of 369 mAh/g. Experimentally, a nanoporous Ge electrode has delivered a capacity of 120 mAh/g.<sup>[20]</sup>

## 3 Challenges and limitation in Si and Ge anodes

Whether the Si or Ge alloying reaction with alkali is anisotropic or isotropic they lead to volume expansion and particle pulverization. The lithiation of Silicon happens preferentially along the <110> direction with a swelling of ≈200% while the <111> direction experiences only

10%. In contrast, germanium has a more flexible lattice that undergoes facile atom rearrangements during lithiation. As a consequence, the volume expansion happens both in the axial and radial direction, resulting in a more uniform and faster lithiation and in a reduction of particle cracking. <sup>[32,73]</sup> For the sodiation and potassiation, given the inconsistencies with the maximum known values for alkali insertion in Si and Ge ( $\text{NaSi}^{[74]}$ ,  $\text{Na}_{0.76}\text{Si}^{[67]}$ ,  $\text{NaGe}^{[69]}$ ,  $\text{Na}_{1.6}\text{Ge}^{[23]}$ ), the information regarding the nature and degree of volume expansion is limited, though it is known to be related with the quantity and size of inserted alkali. <sup>[3,5,6,8]</sup>

Indeed this volume expansion is one of the main challenges for the implementation of Si or Ge in commercial applications. The full lithiated states can expand up to 300%, compromising the stability of the electrode morphology by the formation of cracks and change in the connections with the conductive network. After delithiation, the particle contracts and is unable to return to its pristine state. With the constant expansion/contraction the particles suffer from cracking and pulverization that derive in a fracture/disconnection from the conductive network. <sup>[11]</sup> The pulverized or disconnected particles cannot participate in the electrochemical reaction leading to capacity fading. <sup>[75]</sup> Another limitation is the low initial coulombic efficiency due to the consumption of  $\text{Li}^+$  by the SEI formation during the first cycle, which contributes to the irreversible capacity and depletion of the Li reservoir in the cathode (for a full cell). Moreover the trapping of Li increases upon cycling due to the continuous formation of fresh surfaces in the alloying/dealloying process. To summarize the silicon/germanium electrode failure is due to <sup>[10,11,76]</sup>

i) Large volume changes in bulky films and particles lead to high internal stress causing pulverization of the particles.

ii) Pulverization leads to detachment from the current collector and conductive network, causing isolation of the material, meaning that they no longer contribute to the energy delivered by the electrode.

iii) Unstable and uncontrollable growth of the SEI layer that increases the resistance of the electrode and irreversibly consumes Li. The expansion and contraction is continuously exposing fresh particle surface for the formation of new SEI layer.

Since the volume change cannot be avoided, the key solution is the improvement of the cyclability by preventing the loss of electrical contact between the electrode and the current collector and by stabilizing the SEI layer. Strategies to achieve this goal are the reducing of the operating voltage at the expense of the capacity and the use of composites and nanostructures.

### 3.1 Nanostructures

Limiting the particle size has been proven to be a good strategy to improve cyclability. Indeed, both silicon and germanium have a critical particle size after which the cracks appear. For crystalline silicon this value is limited to 150 nm<sup>[4,8]</sup> while for the a-Si and c-Ge due to their isotropic volume expansion these values are limited to 870<sup>[31,77]</sup> and 620 nm<sup>[33,48]</sup>, respectively. The use of nanostructures appears then as an efficient approach to improve the cyclability since i) their smaller size buffers the volume expansion and their unique architecture minimizes the stress along a specific orientation and avoids cracking or pulverization<sup>[11]</sup>, ii) their high surface area maximizes electrochemical reactions in the electrode but also increases the amount of parasitic reactions<sup>[35]</sup>, their interconnected electrolyte-filled network enables fast ion transport and their structure offers a directional path for fast electron transport.<sup>[78]</sup> Each type of architecture contributes in a different way to the electrochemical performance but has its own limitations, from here the interest of combining them in the electrode design. In the following segment we will revise the characteristics of the most common nanostructures.

**Nanoparticles (NP):** Their smaller size grants a lower associated volume expansion, higher specific surface area and tolerance to tensile stress and improved transport pathways for electrons and ions along the binders or conductive additives. All of these conditions minimize the electrode degradation and improve the cycling performance.<sup>[38,75,76,79]</sup> Nevertheless, the cycling stability is restricted by the limited space to accommodate volume changes, undesirable reactions and excessive formation of SEI in their surfaces.<sup>[79]</sup> In addition, with repeated cycling the NP tend to merge into bigger particles, leading to a decrease in the surface to volume ratio and eventual peeling from the current collector.<sup>[31,80]</sup>

**1D structures:** They distribute the volume expansion along the radial direction, in order to minimize particle cracking and the abundant empty space between the structures serves as a buffer for volume changes. Along the length direction they provide efficient electron transport and intimate contact with the current collector, allowing rapid charge transfer. However their synthesis methods are complicated and expensive, hindering their implementation at large scale.<sup>[10,38,75,81,82]</sup> Examples of these type of structures are the nanowires (NW), which can be grown directly in the current collector eliminating the need for conductive additive or binders. Unfortunately, the NW still can be broken and expose surface to the formation of new SEI layer that will thicken with repetitive cycling limiting the Li<sup>+</sup> transfer.<sup>[76]</sup> Hence, there is a critical diameter (<300 nm) in order to obtain the best performance in terms of coulombic efficiency and cycle life.<sup>[80,83]</sup> The nanowires can be added as active material in a composite containing the binder and the conductive additive, often they result in flexible and robust structures.<sup>[11]</sup> The nanotubes (NT) compared to NW and nanofibers usually bear much higher specific surface area when they possess a hollow structure. This last one helps to buffer the volume expansion, allowing it to be released inward and outward.<sup>[11]</sup> Since the outer and inner parts are exposed to the electrolyte, the diffusion paths for the ions are shorter, but an excessive formation of SEI layer is promoted.<sup>[81]</sup> The length, outer and inner diameters and the



wall thickness are important parameters that determine the electrochemical performance of the NT.<sup>[80]</sup>

**2D structures:** In order to avoid the particle rearrangement due to volume expansion the initial film should have enough void space (interparticle space) to accommodate the changes.<sup>[10]</sup> The film thickness has an impact on the electrochemical performance and in general thinner films perform better due to a better conductivity due to a shorter distance to the current collector.<sup>[11]</sup> For these factors the thin films have limited mass loading and thickness and are only foreseen for microbatteries.<sup>[75,80,81]</sup> Note that films with thicknesses lower than 2.5 $\mu\text{m}$  do not form  $\text{Li}_{15}\text{Si}_4$ .<sup>[80]</sup> Another 2D structures are the nanosheets (NS), due to their low dimensionality they provide fast kinetics for ion transport and buffer the strain generated by the expansion/contraction process. Their large surface area allows an effective contact between the electrolyte and the electrode.<sup>[81]</sup>

**Micron-sized Si(Ge).** Despite the advantages of nanostructures to buffer the volumetric expansion, they depict complex synthesis methods, low mass loading and low coulombic efficiency. Hence it is practical to engineer micrometer silicon with characteristics of the nano-sized one.<sup>[10]</sup> With this approach, the tap density can be increased and as a consequence the volumetric energy.<sup>[38]</sup> This strategy can be implemented either by the introduction of nanopores/nanograins or by the incorporation of nano/micro-meter Si(Ge) in a micrometer host such as graphite or other carbon frameworks.<sup>[11,82]</sup> The pores diminish particle pulverization, serve as buffer for volume changes and facilitate the electrolyte diffusion in the structure; while the composites containing carbon benefit from a better structural stability, enhanced conductivity and stabilization of the SEI layer.<sup>[11,75,79]</sup>

**Prelithiation:** The high surface area of nanoparticles decreases the coulombic efficiency during the first cycle due to irreversible consumption of Li in the formation of the SEI layer, this process depletes the Li reservoirs in the cathode (for a full cell). With the prelithiation an

artificial SEI layer is created that is activated upon contact with the electrolyte, reducing the consumption of Li during the first cycle. <sup>[38]</sup> This process can be performed in three ways; electrochemically by contacting lithium foil with electrolyte-wetted anodes, mechanically by mixing the Si(Ge) with lithium metal powder and chemically by the synthesis of  $\text{Li}_x\text{Si}$  ( $\text{Li}_x\text{Ge}$ ) nanoparticles that are mixed with the rest of the slurry. <sup>[10,82]</sup>

**Composites:** Since it is challenging to tackle all of the Si(Ge) drawbacks by solely morphology control, the design of effective networks is vital for this purpose. The Si(Ge)/core carbon shell, is an interesting structure, in which the void space between the Si(Ge) core and the carbon shell, accommodates the volume changes without deterioration while the SEI layer is stabilized in the surface of the shell. A porous but rigid shell allows to keep the integrity of the conductive network without particle disconnection and provides an active  $\text{Li}^+$  diffusion path and efficient electron transport <sup>[10,38,75]</sup>. Tough, in some cases the volume expansion of the core affects the shell. Hence, the following factors must be considered for an effective design: i) the size of the core (less than 100 nm, to avoid excessive volume expansion), ii) the material of shell should be conductive and electrochemically stable, iii) the synthesis conditions should lead to an uniform, mechanically stable and conductive shell. <sup>[38]</sup> Ideally the shell should be thick enough to provide good mechanical and chemical stability but thin enough to avoid high ionic or electronic resistance. A similar structure is the Yolk-Shell in which the void space is engineered specifically to buffer volume expansion. <sup>[31,38,80]</sup>

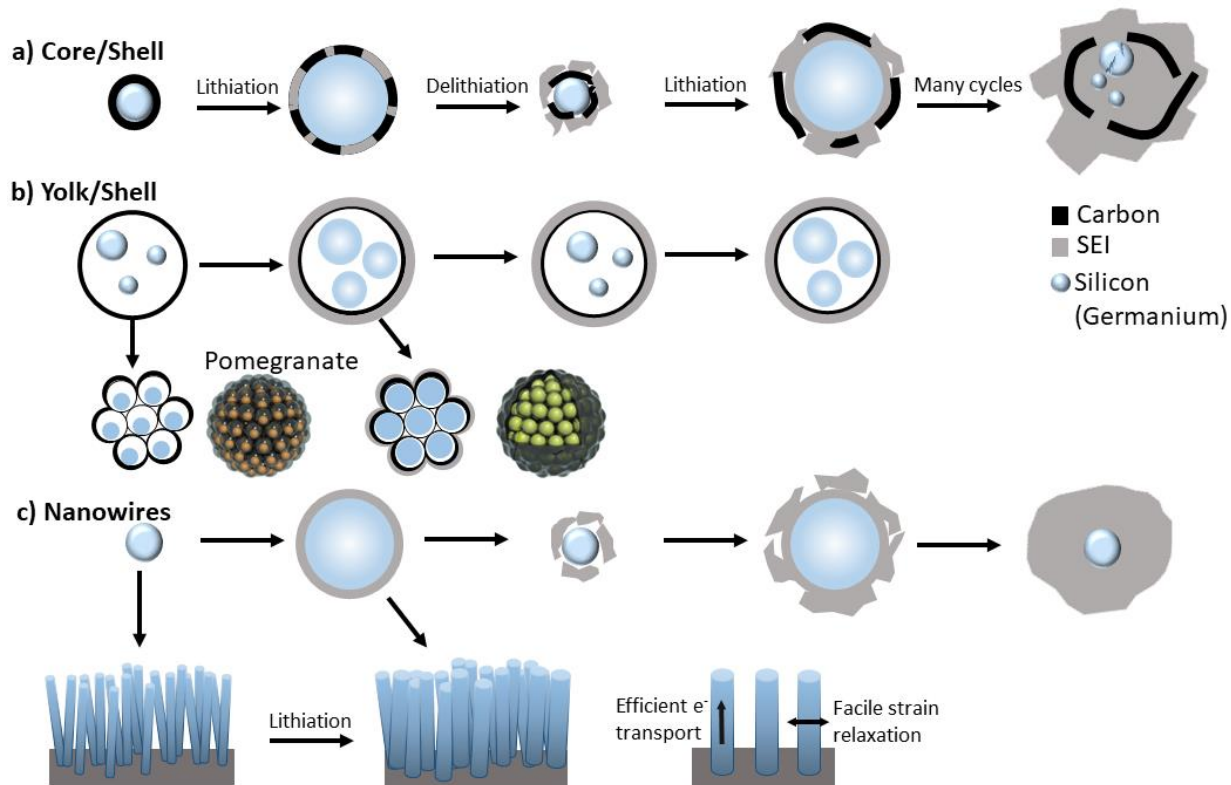


**Figure 7.** Solutions for fundamental problem of Si(Ge) anodes. Volume expansion and contraction of a) Core/shell, b) Yolk shell and the pomegranate assembly and c) Nanowires during lithiation and delithiation. The continued cycling leads to an uncontrolled growth of SEI layer in the core/shell and nanowires while the yolk/shell-type structures are able to stabilize a uniform SEI layer. Adapted from <sup>[10,79]</sup>

**Silicon-graphite composites:** This composite presents a remarkable improvement compared to graphite with good cycling stability and low cost of fabrication. The synergy between Si and graphite increases the capacity and improves the electrical conductivity and stabilizes the SEI layer. Note that the ratio between both components is critical in the electrode design to ensure the benefits from both materials. <sup>[11]</sup>

**Silicon-graphene:** In this composite the Si particles are deposited in between the layers of graphene which can deform easily to accommodate the volume expansion. The graphene layers that are far away from Si particles can reconstruct the graphite network due to van der Waals forces. <sup>[76]</sup> This method presents good mechanical stability and prevents the Si particles to be disconnected from the conducting network; it allows as well the preparation of free

standing electrodes. <sup>[11,76,79,80]</sup> However, since NP tend to aggregate, selecting the ideal matrix that can provide flexibility, high surface area and efficient electron and ion transport is important. <sup>[79]</sup>

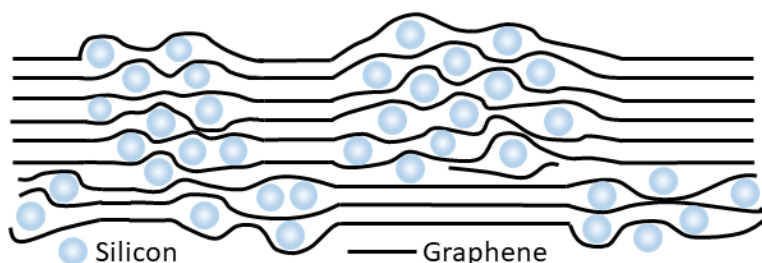


**Figure 8.** Schematic of a Silicon/Graphene composite. Adapted from ref. <sup>[84]</sup>

**Metal alloys:** the use of metal alloys is another alternative to benefit from the desired properties of two or more elements. A very interesting composite is the Si-Ge alloy. Since Ge exhibits a series of advantages over Si, such as faster  $\text{Li}^+$  diffusion, higher electronic conductivity and lower volumetric expansion; the enrichment with Ge affects the rate capability and allows a better capacity retention. <sup>[85,86]</sup> Sn has also demonstrated to contribute to improve the capacity retention of a Si electrode. <sup>[87]</sup>

It is worth to note that most of these approaches are implemented as well for NIB, but despite the similarities between Li and Na, certain functions used for LIB may not work for NIB, because of the different kinetic limitations between the two systems. <sup>[78]</sup> Certain examples include the c-Si core/ a-Si shell composite, in which the c-Si core improves the electronic conductivity whereas the sodium storage occurs in the a-Si shell. <sup>[17]</sup> A porous Si-sponge, in which the synergy between the porous and the amorphous character helps to alleviate the volume expansion and improve Na kinetics, allowing cycling at high C/rates. <sup>[12]</sup> a-Si nano-membranes with enhanced  $\text{Na}^+$  transport kinetics is able to store Na through a pseudocapacitive/bulk mechanism. <sup>[66]</sup> A silicon/graphene and silicon graphite composite alleviates the Na transport limitation issues and improves the electronic conductivity. <sup>[88,89]</sup> Ge

nano-columns improve Na kinetics due to their short diffusion length. <sup>[90]</sup> a-Ge NP supported in Ni nano-pyramids with enhanced cycling stability and rate capability, due to enough space between each pyramid to buffer the volume changes and the intimate contact between Ni and Ge that shorten the diffusion paths. <sup>[68]</sup> The use of a-Ge thin film or porous c-Ge NP in which all the sodiation products are amorphous. <sup>[68,91,92]</sup> Finally the Li activation of Ge NWs, induces amorphization and porosity in the structure, reducing the barrier for nucleation of the Na<sub>x</sub>Ge phase and accelerates the solid state Na diffusion. <sup>[29]</sup> Indeed a-Ge NW can store up to 1.6 Na per Ge (Na<sub>1.6</sub>Ge) due to the high concentration of defects in a-Ge. <sup>[23]</sup>

**Table 4.** Electrochemical performance of some Si anodes for LIB and NIB. Adapted from refs.

[11,17,75,82]

Type of Si(Ge)		Cycling stability		
		Specific capacity (mAh g <sup>-1</sup> )	Cycle number	Current/rate
<b>LIB</b>				
Nanosized Si (Ge)	Si Nanoparticles	1180	500	3 Ag <sup>-1</sup>
	Ge Nanoparticles	1100	100	C/10
	Hollow Si	1420	700	C/2
	Porous Si	1200	600	C/2
	Si Nanowire	3500	20	C/5
	Ge Nanowire	1000	20	C/20
	Si Nanofiber	1821	1000	C/5
	Si Nanotube	2000	50	C/5
	Ge Nanotube	1002	50	C/5
	Si nanofilm	3000	1000	12C
Micrometer Si (Ge)	3D porous Si	2800	100	1C
	Pomegranate-like Si	1160	1000	C/2
Si (Ge)/C composites	Simple Ge/C	700	50	0.15 Ag <sup>-1</sup>
	Simple Si/C	1200	30	C/10
	Core-shell Si/C	1490	1000	C/4
	Yolk-shell Si/C	1500	1000	1C
	Si/graphene	840	300	1.4 A g <sup>-1</sup>
	Ge/graphene NW	1059	200	4C
Other composites	Si/conductive polymer	550	5000	6 A g <sup>-1</sup>
	Si-Ge alloy	1600	50	2C
<b>NIB</b>				
Nanosized Si	a-Si	270 (after 1 <sup>st</sup> )	100	20 mA g <sup>-1</sup>

(Ge)	Nanoparticle a-Si thin film	cycle) 600 (after 1 <sup>st</sup> cycle)	(248 mAh g <sup>-1</sup> ) 100 (240 mAhg <sup>-1</sup> )	C/10
Si(Ge)/C composite	Si/C fiber	283 (after 1 <sup>st</sup> cycle)	200 (298 mAh g <sup>-1</sup> )	50 mA g <sup>-1</sup>

### 3.2 Electrolyte formulation and additives

In addition to the electrode architecture and composition, other features have to be considered to improve the performance of Si (Ge) anodes. One of them is the electrolyte formulation since it is related to the formation of the SEI layer that is expected to inhibit further side electrochemical reactions on the surface of the electrodes and to guarantee a good cycle life via effective ion transport. <sup>[75]</sup> However, the alloying reaction promotes a continuous and excessive SEI formation due to its facile detachment from the particles surface during the expansion/contraction process and the particle cracking that exposes new surface area. This uncontrolled growth of SEI layer impedes the transport of ions and increases the resistance of the electrode. <sup>[75]</sup> In general the stability of the SEI layer depends on the choice of salts, solvents and additives. <sup>[76]</sup> The SEI layer derived from carbonate solvents is composed of polymeric and oligomeric organic units and it is semipermeable to the electrolyte components, meaning that it is continuously decomposed with little passivation effect. <sup>[11,76]</sup>

Hence, an efficient approach to stabilize this SEI layer is the use of additives, which most of the times are designed to be consumed during the initial formation the SEI layer, but can serve also to improve the electrochemical stability window of the electrolyte, or to enhance the safety (flame retardants). <sup>[93]</sup> Common additives include vinyl carbonate (VC), fluoroethylene carbonate (FEC) or Lithium bis(oxalate)borate (LiBOB). <sup>[11,81]</sup> Both FEC and VC reduce before the carbonates providing an initial protective layer on the particle surface. VC decomposes into polycarbonates at about 1 V vs Li/Li<sup>+</sup>, the presence of double bonds in its structure rend it is more susceptible to reduction. <sup>[11,94]</sup> FEC decomposes at 1.3 V vs Li/Li<sup>+</sup> into a passivating layer that is much more compact resulting in a lower mass transfer resistance and improved

capacity retention. <sup>[3,11,93]</sup> FEC decomposes into polyenes and a high concentration of  $\text{Li}_2\text{O}$  which prevents the diffusion of HF through the SEI. <sup>[93]</sup> It promotes the formation of Li-F and Si-F (Ge-F) bonds that are much stronger and give more stability to the SEI layer, compared to Si-C (Ge-C) or Si-O (Ge-O) bonds that are constantly decomposing and reforming if there is no additive. However, if FEC is used in excessive quantities, the formation of HF and LiF is boosted, causing cathode dissolution, consumption of Li reservoirs and increase of the irreversible capacity. <sup>[10,11,94]</sup> It is crucial then to optimize the additive content and to use mixtures (VC+FEC) with synergetic effects that impact the electrode performance. <sup>[94]</sup>

For Sodium and potassium, given their different reactivity with the electrolyte solvents, the composition of the SEI layer differs from their Li analogue. For Na a lower quantity of oxygenated or organic species is found, being mainly composed of  $\text{Na}_2\text{CO}_3$  and alkyl carbonates  $\text{ROCO}_2$ . Since the Lewis acidity of Na is lower than Li, the coulombic interaction of  $\text{Na}^+$  ions with negatively charged species or lone pairs is weaker, as a result the solubility of the electrolyte decomposition products is higher for NIB. <sup>[3,95-97]</sup> Therefore the use of additives is crucial to avoid further SEI dissolution and electrolyte decomposition. <sup>[3,98]</sup> For potassium, certain electrolytes are suitable for the anode but not for the cathode, due to composition of the SEI layer on top of the K surface (for half cells). For most of the anodes the KFSI salt has been found to be the most stable. The carbonate based solvents allow reversible cycling whereas the glymes-based present systematic failure. <sup>[99]</sup> Whether the additives improve the performance or not is not clear yet <sup>[5]</sup>. In any case, in order to avoid undesired reactions of K with the electrolyte, full cell test must be implemented. <sup>[99]</sup>

### 3.3 Binder

The role of the binder is to keep all the particles together, attach them to the current collector and alleviate the stress induced during volume changes maintaining the mechanical stability of the whole electrode. Polyvinylidene fluoride (PVDF) is one of the most common binders for different technologies, but due to the lack of polar functional groups it only offers weak van

der Waals interactions that are not sufficient to maintain the integrity of the electrode. <sup>[11,76,81]</sup> On the contrary other binders such Carboxymethyl cellulose (CMC), poly acrylic acid (PAA) or Sodium alginate contain polar groups that interact strongly with the hydroxide groups on the particle surface via hydrogen or covalent bonding, improving the adhesion. <sup>[100,101]</sup> These binders are soluble in water, meaning that the slurry can be prepared in aqueous media, which is more environmentally friendly compared to PVDF processing in N-Methyl-2-pyrrolidone (NMP). <sup>[11,76,80,81]</sup> Nonetheless, during the volume expansion process the integrity of the binder can be compromised. The polymer chains can slide, isolating the active material particles from the conductive network, a chain crosslinking can address this issue. <sup>[81]</sup> In this sense, the use of self-healing binders is of great interest since they can repair spontaneously the mechanically destruction of the electrode, thanks to the re-association of hydrogen bonds.<sup>[10]</sup> Another concept is the use of conductive binders that ensure the electrical connectivity of all the particles even after the particle pulverization due to volume changes. <sup>[31]</sup> **(Figure 9)**

Finally, in order to improve the contact between the current collector and the active material to decrease the electrical resistance and improve the cycle life, a porous or rough treatment by sandpaper and chemical or electrochemical etching of the current collector is suggested. <sup>[81]</sup>

For further reading about the challenges and strategies for the implementation Si and Ge anodes reader can be referred to <sup>[10,11,31,38,81,82]</sup>

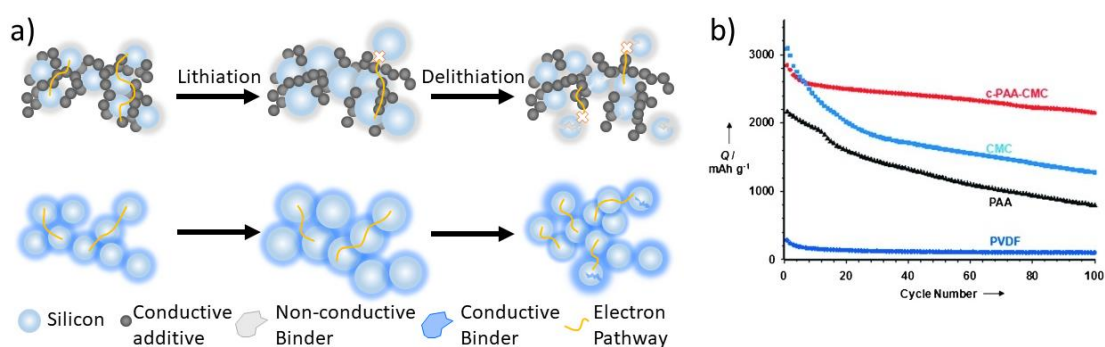


**Figure 9.** Schematic of a Si electrode with non-conductive binder (e.g. PVDF) and conductive additive (e.g. Carbon black) and with conductive polymer with dual functionality as conductor



and binder. Adapted from ref. [102]. b) Capacity vs cycle number for a Silicon anode with different types of binder. [103]

## 4 Zintl Phases

This family of compounds have been known for a long time, but their applications in batteries are very recent. The following section comprises an extensive explanation of the nature, properties, versatility and application of the Zintl phases.

### 4.1 The Zintl-Klemm Formalism

The Zintl phases are named after Eduard Zintl who in 1929 studied a family of compounds in which one component is a highly electropositive material and the other is an element located in the right side of the so-called the Zintl boarder; today known as semimetals, metametals or metalloids. [104] (**Figure 10**) In Zintl phases the valence electrons are formally transferred from the electropositive to the more electronegative component, the anions do not achieve an electronic octet rule as isolated species but may rather bond to each other, forming cationic and anionic frameworks. The versatility of the Zintl phases arises from the characteristics and interactions between these frameworks, resulting in an enormous variety of crystal structures, ranging from cluster compounds to extended solids, in which certain physical and chemical properties can be tuned. [105,106]

The Zintl line defined by Zintl (red) and Klemm (blue)

1 H hydrogen 1.008	2 He helium 4.0026											13 B boron 10.81 (10.806, 10.821)	14 C carbon 12.01 (12.009, 12.012)	15 N nitrogen 14.01 (14.006, 14.008)	16 O oxygen 16.00 (15.999, 16.000)	17 F fluorine 18.998	18 Ne neon 20.180
3 Li lithium 6.94 (6.938, 6.947)	4 Be beryllium 9.0122											13 Al aluminium 26.982	14 Si silicon 28.086 (28.084, 28.086)	15 P phosphorus 30.974	16 S sulfur 32.06 (32.059, 32.076)	17 Cl chlorine 35.45 (35.446, 35.457)	18 Ar argon 39.95 (39.962, 39.963)
11 Na sodium 22.990	12 Mg magnesium 24.30 (24.304, 24.307)	3 Sc scandium 44.956	4 Ti titanium 47.867	5 V vanadium 50.942	6 Cr chromium 51.996	7 Mn manganese 54.938	8 Fe iron 55.845(2)	9 Co cobalt 58.933	10 Ni nickel 58.693	11 Cu copper 63.546(3)	12 Zn zinc 65.38(2)	31 Ga gallium 69.723	32 Ge germanium 72.630(8)	33 As arsenic 74.922	34 Se selenium 78.971(8)	35 Br bromine 79.901, 79.907	36 Kr krypton 83.798(2)
19 K potassium 39.098	20 Ca calcium 40.078(4)	21 Sc scandium 44.956	22 Ti titanium 47.867	23 V vanadium 50.942	24 Cr chromium 51.996	25 Mn manganese 54.938	26 Fe iron 55.845(2)	27 Co cobalt 58.933	28 Ni nickel 58.693	29 Cu copper 63.546(3)	30 Zn zinc 65.38(2)	49 In indium 114.82	50 Sn tin 118.71	51 Sb antimony 121.76	52 Te tellurium 127.60(3)	53 I iodine 126.90	54 Xe xenon 131.29
37 Rb rubidium 85.468	38 Sr strontium 87.62	39 Y yttrium 88.906	40 Zr zirconium 91.224(2)	41 Nb niobium 92.906	42 Mo molybdenum 95.95	43 Tc technetium 98.906	44 Ru ruthenium 101.07(2)	45 Rh rhodium 102.91	46 Pd palladium 106.42	47 Ag silver 107.87	48 Cd cadmium 112.41	81 Tl thallium 204.38, 204.38	82 Pb lead 207.2	83 Bi bismuth 208.98	84 Po polonium	85 At astatine	86 Rn radon
55 Cs caesium 132.91	56 Ba barium 137.33	57-71 lanthanoids	72 Hf hafnium 178.49(2)	73 Ta tantalum 180.95	74 W tungsten 183.84	75 Re rhenium 186.21	76 Os osmium 190.23(3)	77 Ir iridium 192.22	78 Pt platinum 195.08	79 Au gold 196.97	80 Hg mercury 200.59	81 Tl thallium 204.38, 204.38	82 Pb lead 207.2	83 Bi bismuth 208.98	84 Po polonium	85 At astatine	86 Rn radon

**Figure 10.** Periodic Table showing the Zintl border according to Zintl (red) and to Klemm (blue). [107]

Zintl defined some rules in order to distinguish the Zintl phases from intermetallics. A Zintl phase should; <sup>[105]</sup>

- i) Contain an alkali, alkaline-earth metal or p-element that is a metal, semimetal or small bandgap semiconductor.
- ii) Have electrochemically balanced or closed-shell compounds, meaning that the number of electrons provided by the constituting elements is equal to the number of electrons needed to form a covalent bond.
- iii) Have a well-defined relationship between the chemical (geometrical) and the electronic structure.
- iv) Be semiconductors (band gap < 2eV) or poor conductors.
- v) Show diamagnetism or weak temperature dependent paramagnetism (Pauli paramagnetism).
- vi) Be brittle

Since a vast number of compounds that do not follow all the Zintl rules, during the course of the years the definition of Zintl phases has changed and adapted. Wilhelm Klemm extended the Zintl concept through the pseudoatom approach in which he studied isoelectronic Zintl anions. This is, after receiving the electrons from the electropositive metal, the electronegative will behave like the isoelectronic neutral atom at its right. <sup>[105]</sup> In 1980 Von Schnering extended the Zintl-Klemm concept from an 8N rule to a 18 e<sup>-</sup> one, not only to allow the study of transition metal compounds but also to prove that in some phases both concepts can work simultaneously. <sup>[104]</sup> Additional extension of the Zintl Klemm formalism have been proposed by Miller, Mooser and Pearson <sup>[108]</sup>, Corbett <sup>[109,110]</sup>, Van der Lugt <sup>[111]</sup> and Nesper <sup>[104,107,112]</sup> and Belin <sup>[113]</sup>.

Since the discovery of the Zintl phases, several compounds have been successfully synthesized and characterized.

## 4.2 Structural diversity of Zintl phases

The huge structural variety of Zintl phases is determined by the size and interactions of cations and anions. In other words, different structures varying from 0D clusters, 1D wires to 2D layers can be obtained from the same anion by changing the stoichiometry or the cation size. For example, in layered  $\text{CaSi}_2$  each Si is bonded to other three Si atoms, giving 4 + 3 valence electrons and the octet rule is completed by the electron donated from the Ca. This structure is analogous to the 3D bulk Si, but all the bonds along the [111] direction have been replaced by  $\text{Ca}^{2+}$  cations. If the stoichiometry is changed to  $\text{CaSi}$ , then each Si is bonded to only two Si atoms, forming zig-zag wires, here each Si atom has 4+2 valence electrons and the octet rule is completed by 2 electrons from the  $\text{Ca}^{2+}$ . If the  $\text{Ca}^{2+}$  is replaced by a monovalent cation, like in  $\text{KSi}$ ,  $\text{NaSi}$ , each Si atom is bonded to other three Si atoms forming isolated  $[\text{Si}_4]^{4-}$  tetrahedra, this gives 4+3 valence electrons, and the octet rule is completed by one electron from the cation. **Figure 1111** <sup>[114]</sup> This tetrahedral unit  $(\text{X}_4)^{4-}$  similar to  $\text{P}_4$  and  $\text{As}_4$  and can be found in alloys of Si, Ge, Sn, Pb (M) with Na, K, Rb, Cs but not for Li. This effect is related to the size of the cation, as the size increases the metal atoms are more separated one from each other, reducing their interactions, compared to a  $\text{Li}_x\text{M}$  mixture, and in order to decrease their mutual distances and bond energies, they prefer to cluster together. <sup>[111]</sup>

Other type of Zintl phases are the cage-like clathrates, composed of tetravalent group 14 (Si, Ge, Sn and their mixtures) and trivalent group 13 elements as host structure. The guest atom (electropositive metal) is located in the cavities of the network and balances the electron deficiency by the formal charge transfer. The most common types of clathrate are Type I with the formula  $\text{A}_8\text{E}_{46}$  and Type II with  $\text{A}_{24}\text{E}_{136}$ . <sup>[115]</sup> Another type of structures are the allotropes, composed of different arrangements of the same element that determine the specific properties of the material, examples are the allo-Ge and allo-Si. The first one is obtained from oxidation of  $\text{Li}_7\text{Ge}_{12}$ , a phase with two dimensional polyanionic  $[\text{Ge}_{12}]^{7-}$  separated by Li atoms. The second one from  $\text{Li}_3\text{NaSi}_6$  which has polyanionic layers of  $[\text{Si}_6]^{4-}$  separated by Li and Na

atoms. In both cases the alkali is extracted while preserving the anionic structure. <sup>[116]</sup> These structural versatility opens a field of study, since the material properties can be changed in function of the desired application (optoelectronics, spintronic, magnetic, catalytic activity, etc.)<sup>[114]</sup>.

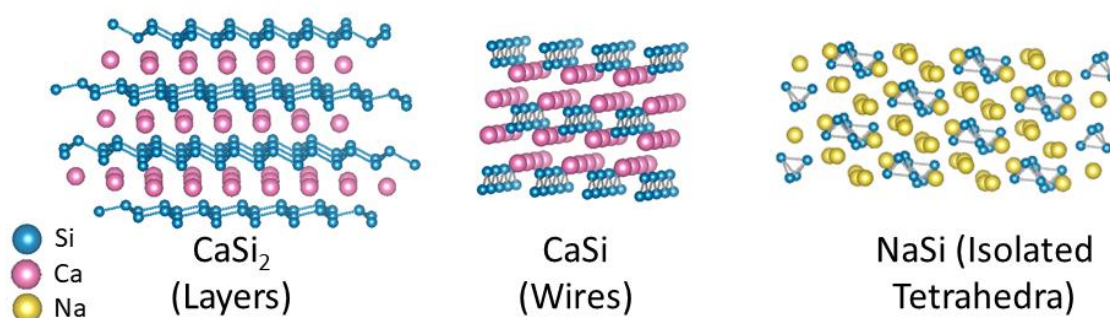


**Figure 11.** Structural models for CaSi<sub>2</sub> (layers), CaSi (wires) and NaSi (isolated tetrahedra).

#### 4.2.1 Binary Zintl phases

**Li<sub>x</sub>M (M=Si, Ge):** Lithium based Zintl phases present different characteristics compared to the heavier alkali metal homologues, even with the same stoichiometry they exhibit completely different structures. The main reason is the Li high electron affinity, strong polarizing power and smaller size, which condensate the Zintl anions around the Li<sup>+</sup>. <sup>[107]</sup> For example, the LiM (1:1) consists of infinite [X] linkages while the Na, K, Rb, Cs analogues ideally form X<sub>4</sub><sup>4-</sup> tetrahedra. Interestingly, the lithiated compounds with group 14 elements are mostly isotypic, meaning that Si can be replaced by Ge up to some extent. <sup>[107]</sup> Most of the Li-Si and Li-Ge phases do not follow the Zintl-Klemm concept. Both Si and Ge are not electronegative enough to completely strip all the Li atoms of their electrons and the charge transfer is not complete. At low lithium contents the compounds behave like Zintl phases but as the Li ratio increases the standard electron counting rules fails. <sup>[107,117]</sup> Examples of compounds that do not follow the electron counting rules are almost all lithium silicides and germanides, Li<sub>12</sub>Si<sub>7</sub>, Li<sub>13</sub>Si<sub>4</sub>, Li<sub>21</sub>Si<sub>5</sub>, Li<sub>12</sub>Ge<sub>7</sub>, Li<sub>9</sub>Ge<sub>4</sub>, Li<sub>13</sub>Ge<sub>4</sub>, Li<sub>14</sub>Ge<sub>4</sub> and Li<sub>21</sub>Ge<sub>5</sub> except the Li<sub>7</sub>Ge<sub>12</sub>, LiGe and LiSi. The electronic structure of all these compounds can be understood if the concept of an additional electronic state corresponding to a cage orbital is used. A cage orbital corresponds to metal (Li) electronic

state being delocalized uniformly over other Li atoms that envelops certain Zintl ions. <sup>[107,117]</sup>  
Note that the composition of several silicides and germanides have been revised in the literature after the first time they were reported, some of them are not included in the phase diagram, since there is still controversy about their true composition. <sup>[116]</sup>

In the next segment we will revise the properties of some of the most common  $\text{Li}_x\text{M}$  phases.

**(Figure 12)**

*LiM*. Among the LiSi series several metastable phases with same composition and pressure dependent atomic arrangements can be found. Examples are the Li tetrahedral in a three-fold coordinated Si network, layered structure with two dimensional (nontetrahedrally) four-fold coordinated Si with Li intercalated in the sheets, the buckled Si sheets with eight and four-rings and the Li intercalated silicene (Si sheets with six-member honeycombs). <sup>[55]</sup> Some of the previously listed structures are isostructural to LiGe. <sup>[105,118]</sup> At lower pressures three-dimensional three-fold silicon/germanium networks prevail, at high densities both Si and Ge exhibit sheets. <sup>[55]</sup>

*Li<sub>12</sub>M<sub>7</sub>*. These compounds contain planar five membered rings and star-trigonal planar  $\text{M}_4$ . They have a cage orbital that helps to stabilize the structure in a planar configuration. <sup>[107,117,119,120]</sup>

*Li<sub>7</sub>M<sub>3</sub>/Li<sub>9</sub>M<sub>4</sub>*. The  $\text{Li}_7\text{M}_3$  and  $\text{Li}_9\text{Ge}_4$  phases have double bonded  $\text{X}_2$  dumbbells and electrons in cage orbitals distributed over the surrounding Li atoms. <sup>[41,107,117]</sup>

*Li<sub>13</sub>M<sub>4</sub>/Li<sub>15</sub>M<sub>4</sub>*. In the  $\text{Li}_{13}\text{Si}_4$  half of the atoms are in Si dumbbells and the other half are isolated atoms surrounded by Li atoms. The  $\text{Li}_{13}\text{Ge}_4$  crystallizes in a different type of structure with a higher ratio of isolated Ge atoms per dumbbells. <sup>[55,107,121]</sup> The  $\text{Li}_{15}\text{M}_4$  phases are isostructural for Si and Ge and are composed of only isolated M atoms surrounded by Li atoms. They do not satisfy the electron counting rules and are electron deficient. <sup>[18,55,57,107]</sup> These phases can be obtained electrochemically or by mechanical synthesis,  $\text{Li}_{15}\text{Si}_4$  is metastable and decomposes

into other crystalline phases at  $\approx 170^\circ\text{C}$ , while  $\text{Li}_{15}\text{Ge}_4$  is thermodynamically stable and melts at  $720^\circ\text{C}$ . [55,57,121]

$\text{Li}_{21}\text{M}_5/\text{Li}_{22}\text{M}_5$ . Both phases are composed of isolated M atom surrounded by Li atoms. The  $\text{Li}_{22}\text{Si}_5$  and  $\text{Li}_{21}\text{Si}_5$  have two and one extra electron respectively, these electrons are distributed in cage orbitals. Since the first report of the  $\text{Li}_{22}\text{Si}_5$  [46] there has been controversy about its true composition, which was later revised to  $\text{Li}_{21}\text{Si}_5$  [46,47]. It was determined that both phases are temperature dependent and have similar XRD patterns; with  $\text{Li}_{21}\text{Si}_5$  being stable at room temperature whereas  $\text{Li}_{22}\text{Si}_5$  only at  $415^\circ\text{C}$ . [47,55,117]

$\text{Li}_{17}\text{M}_4$ . There has been great controversy regarding the composition of the Li-rich phases, as a result some of them do not figure in the Li-Si or Li-Ge phase diagrams. The  $\text{Li}_{17}\text{M}_4$  structure is closely related to the  $\text{Li}_{21}\text{M}_5$  only differing in the occupation of one fourfold special position, in both  $\text{Li}_{17}\text{Si}_4$  and  $\text{Li}_{17}\text{Ge}_4$  the positional parameters are almost identical. Some authors claim that the  $\text{Li}_{17}\text{M}_4$  is the real composition of  $\text{Li}_{21}\text{M}_5$ . [121,122]

As observed there are many Lithium silicides and germanides that have the similar composition and formation energies, in a LIB the system does not necessarily have the time to equilibrate thermodynamically. In general it has been observed that upon lithiation both Si and Ge exhibit dumbbells and as the lithium concentration increases these are broken into isolated atoms. The dumbbells break at lower concentrations for the Li-Ge system than in Li-Si. Since these dumbbells have been observed for ground-state and metastable phases, it is likely to find them in LIB. [55]

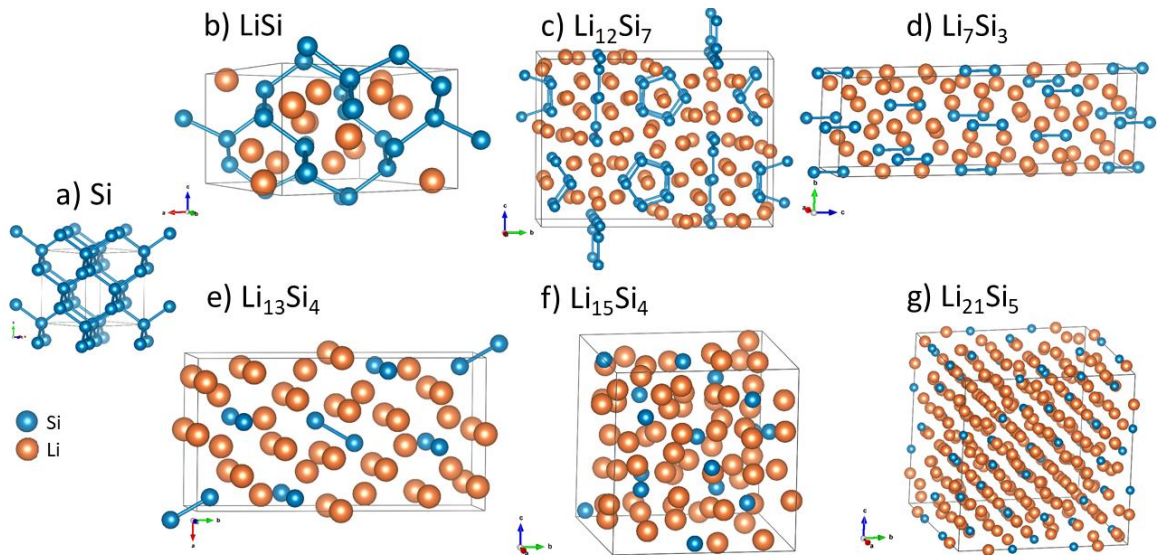


**Figure 12.** Structural representations of a) Si, b) LiSi, c)  $\text{Li}_{12}\text{Si}_7$ , d)  $\text{Li}_7\text{Si}_3$ , e)  $\text{Li}_{13}\text{Si}_4$ , f)  $\text{Li}_{15}\text{Si}_4$  and g)  $\text{Li}_{21}\text{Si}_5$

**$\text{Na}_x\text{M}$  ( $\text{M}=\text{Si}, \text{Ge}$ ).** The NaSi and NaGe are monoclinic and contain isolated  $[\text{Si}_4]^{4-}$  or  $[\text{Ge}_4]^{4-}$  clusters surrounded by four alkali metal cations, each  $\text{Na}^+$  donates one electron to the  $[\text{X}_4]^{4-}$  unit. <sup>[123]</sup> The Si<sup>-</sup> and Ge<sup>-</sup> are pseudoelements of group 15 since they are isoelectronic with As and P and adopt the same tetrahedral units like in  $\text{P}_4$  and  $\text{As}_4$ . <sup>[107,123]</sup> In contrast LiSi has a different structure formed from interpenetrating sheets and does not contain isolated clusters.

[118]

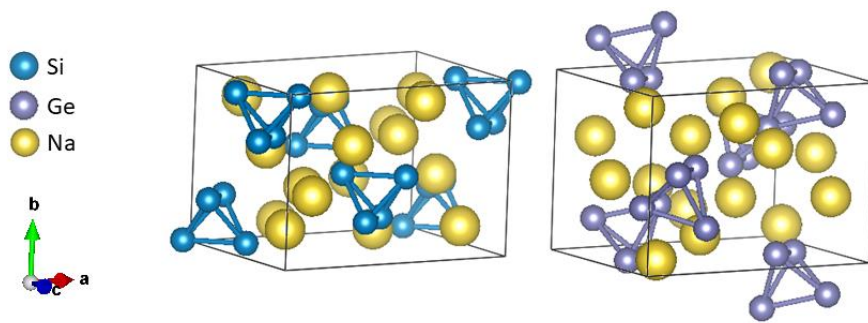


**Figure 13.** Structural representations of NaSi (right) and NaGe (left).

**$\text{Ca}_x\text{M}_y$  ( $\text{M}=\text{Si}, \text{Ge}$ ).**

The group 12, 13 and 14 elements can form extended covalently bonded networks of different dimensionality depending on their coordination. The  $\text{AX}_2$ -type Zintl phase with

A=electropositive divalent element (Ca, Sr, Ba, Eu) and X=group 12, 13 or 14 element stabilizes in structures like orthorhombic  $\text{KHg}_2$ , hexagonal  $\text{CaIn}_2$ , Hexagonal  $\text{AlB}_2$ , cubic  $\text{MgCu}_2$ , hexagonal  $\text{MgZn}_2$  or  $\text{MgNi}_2$ .<sup>[105]</sup> These phases typically form 0D clusters, 1D wires or 2D sheets of the main element held by the cation; the dimensionalities can be tuned by varying the stoichiometry or the size ratio of the anion and the cation. The layered Zintl phases are very sensitive to their stacking sequences and the nature of the surrounding layers, in this sense understanding the interactions of neighboring atoms can lead to exotic forms of the material.<sup>[124]</sup> For instance, many layered materials have polymorphs with different stacking sequences that exhibit different properties.<sup>[104]</sup>

Group 14 elements are characterized by the formation of 2D compounds ( $\text{AlB}_2$ -type), like graphene, consisting of  $\pi$ -bonded honeycomb lattices of carbon atoms. Si and Ge, due to their larger atomic sizes do not form this type of  $\pi$ -bonding, their atomic bonding distances are longer thus each atom would preferentially bond to another ligand than to form a  $\pi$ -bond with its neighbor. This issue leads to the formation of puckered  $[\text{Si}]_n$  and  $[\text{Ge}]_n$  layers separated by monolayers of the alkali cation, like in  $\text{CaSi}_2$  and  $\text{CaGe}_2$ .<sup>[125]</sup> These basic units are isoelectronic and structural analogous to black phosphorous, grey arsenic or bismuth.<sup>[107]</sup> One of the most impressive features of these 2D phases is their ability to undergo topotactic alkali deintercalation to form another type of van der Waals materials, the  $\text{sp}^3$ -hybridized group 14 graphene/graphane analogues.<sup>[125]</sup>

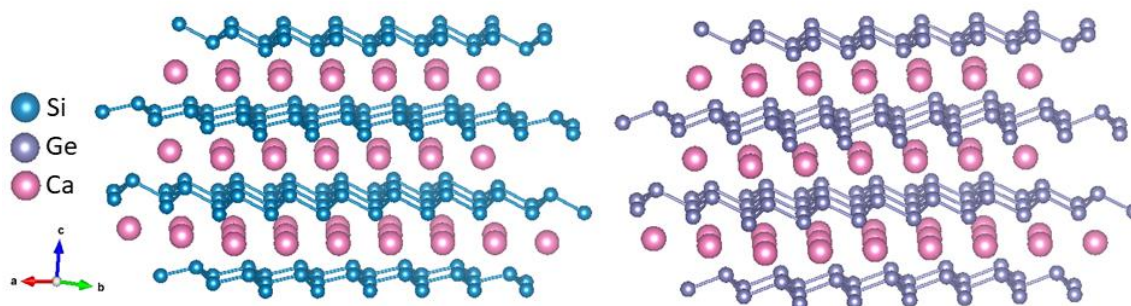
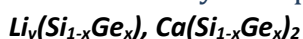


**Figure 14.** Structural representations of  $\text{CaSi}_2$  (right) and  $\text{CaGe}_2$  (left).



## 4.2.2 Ternary Zintl phases



Some Zintl phases can be stabilized by the introduction of a second anion if a common array of cations is supplied. These phases are known as the double salts, and originally appeared by the introduction of oxygen impurities in the lattice. The stabilization of binary compound is done by different phase formation and it is only possible if the distances between cation-anion are not too small. In fact, the presence of the cation plays an important role, in many cases the binary phase diagram for the electronegative (semi)metals pair does not predict the existence of any compound in the solid state (e.g. Zn-Sn, Al-Ge, Al-Sn), nevertheless the introduction of an active phase or cation stabilized new phases (e.g. Na-Zn-Sn, Sr-Al-Ge, Ae-Al-Sn (Ae=alkaline earth metal)). As the combination of electronegative elements approaches the border line between the triel elements (B, Al, Ga, In, Tl) and tetrel elements (C, Si, Ge, Sn, Pb) the resulting structures begin to deviate from the Zintl-Klemm formalism.<sup>[105]</sup> It has been demonstrated that certain ternary systems behave differently depending on their electronic structure changing the chemical bonding; in some cases, the system prefers to adopt a two-phase configuration rather than an electronic and structural distortion.<sup>[105]</sup> Since Si and Ge are miscible, the existence of  $\text{Si}_{1-x}\text{Ge}_x$  compounds with Li and Ca is possible.

## 4.3 Zintl phases in batteries

In the previous segment it was possible to have a brief picture of the immense structural variety of Zintl phases, hence their use in batteries is coherent. Different Si and Ge Zintl phases have been used to prepare alternative structural organisation by chemical extraction of the alkali. E.g. the delithiation of c- $\text{Li}_{15}\text{Si}_4$  that leads to an a-Si and the delithiation of  $\text{Li}_{12}\text{Si}_7$ ,  $\text{Li}_7\text{Si}_3$  and  $\text{Li}_{13}\text{Si}_4$  that generates layered Si.<sup>[126]</sup> Amorphous Si nanoparticles can be prepared as well from the NaSi Zintl phase. Similarly, Ge nanoparticles can be obtained from  $\text{Na}_{12}\text{Ge}_{17}$ .<sup>[127,128]</sup> The previously mentioned phases showed superior Li storage compared to their bulk counterparts.<sup>[126-128]</sup> Another example is the preparation of allo-Si or allo-Ge from  $\text{Li}_3\text{NaSi}_6$  and

Li<sub>7</sub>Ge<sub>12</sub>, respectively <sup>[116]</sup>; and the layered Si and Ge obtained from CaSi<sub>2</sub> and CaGe<sub>2</sub>, respectively. These last ones will be studied in detail in the following chapters.

#### 4.3.1 Xnes, Xanes (X=Si,Ge)

The Xnes makes reference to the single-element layered graphene analogues made from group 14 and group 15 elements. Their ligand-functionalized derivatives are known as Xanes.

##### *Silicene/Siloxene*

As observed in the previous sections, silicon can show an impressive versatility in terms of structural variety and specific properties. Likewise carbon, it has the ability to form layered structures; like the buckled sheet based on the bulk Si (111) structure with honeycomb lattice and sp<sup>3</sup> hybridization and the weakly corrugated graphene analogue with mixed sp<sup>2</sup>-sp<sup>3</sup> hybridization. <sup>[129]</sup> In order to understand the formation of these structures it is convenient to review the similarities between carbon and silicon, listed in the following **Table 4**. <sup>[129,130]</sup>

**Table 5.** Comparison of the properties of carbon and silicon

Carbon	Silicon
Group 14	Group 14
Four valence electrons in the outermost shell Four valence orbitals Formation of four two-electrons covalent bonds	Four valence electrons in the outermost shell Four valence orbitals Formation of four two-electrons covalent bonds
Pauling electronegativity X = 2.55 for C and 2.2 for H	Pauling electronegativity X = 1.90
Polarization of the bond C-H C <sup>δ-</sup> -H <sup>δ+</sup>	Polarization of the bond Si-H Si <sup>δ+</sup> -H <sup>δ-</sup>
Strong C-H bonds	Reactive Si-H bonds
Large energy difference between s and p orbitals (10.60 eV) originating sp, sp <sup>2</sup> and sp <sup>3</sup> hybridization.	Smaller energy differences between the s and p orbitals (5.66 eV), lower hybridization energies. Silicon tends to use all its three p orbitals resulting in sp <sup>3</sup> hybridization.
No energetically accessible d orbitals to expand its coordination or valence shell.	d orbitals (or other virtual orbitals) are energetically low allowing Si to expand its coordination sphere from four to five or six.
Small atomic size, efficient π-π overlap, formation of double and triple bonds. C-C, C=C and C≡C bond distances are 1.54, 1.34 and 1.20 Å respectively.	Larger atomic size, poor π-π overlap Si-Si and Si=Si bond length are 2.35 and 2.16Å respectively.
C=C results in planar structures	Si=Si non stable in planar structure, often folded or twisted.

As observed in the previous table Si and C are very alike, indeed the silicon equivalent of graphene, the silicene, was predicted more than 50 years ago. However, this Si monolayer is not stable and cannot be found in nature. Despite graphene which has a  $sp^2$  hybridization leading to planar structures, in silicene due to the bigger size of Si, a mixed  $sp^2/sp^3$  hybridization is favored resulting in a buckled structure while the planar one is energetically non-favored. <sup>[131–133]</sup> Consequently, the synthesis of free-standing silicene has not been achieved, although it has been grown on metallic substrates. The lifetime of this material is very short and oxidizes rapidly outside the ultra-high vacuum. <sup>[132,134–136]</sup>

Silicene is of particular interest due to its unique physical and chemical properties, strikingly different from the bulk ones, modifiable by chemical doping. Because of the 2D nature, charge carriers are highly mobile. This property is of particular interest for applications like transistors, photo-detection, biomedical imaging, optoelectronic devices, quantum information technology remote sensing, and optical communications, among others. <sup>[132,137]</sup>

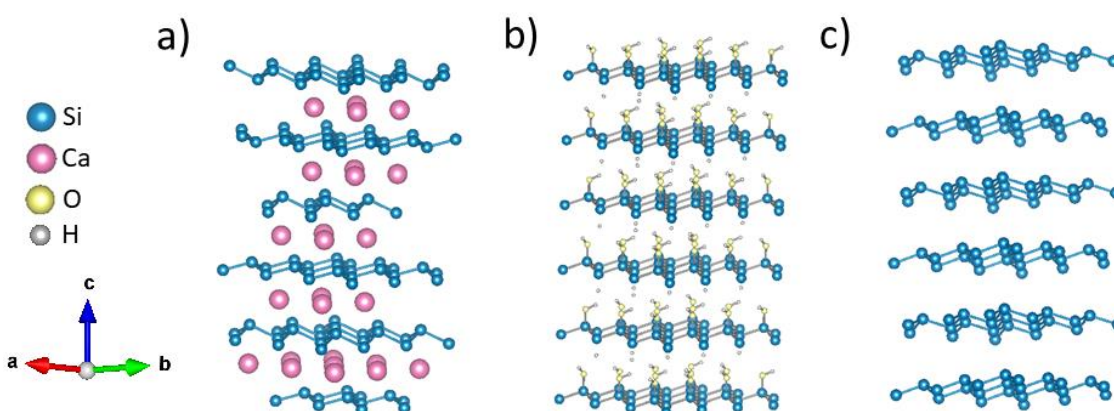
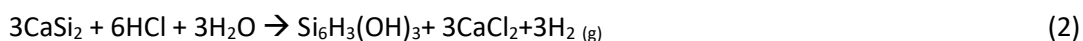


**Figure 15.** Structural representations of a)  $CaSi_2$ , b) Siloxene ( $Si_6H_3(OH)_3$ ) and c) Silicene.

Silicene can be functionalized; the hydrogen terminated silicene (polysilane) has higher stability and it is a free standing sheet. <sup>[138]</sup> The adsorption and desorption of hydrogen is reversible and can be used for controlled hydrogen storage. <sup>[132]</sup> The chemisorption and intercalation of species like Li, Na, Mg in the layers has been theoretically studied. <sup>[136,139]</sup>

Indeed, Li can be reversibly adsorbed in both sides of a Silicene layer with no structure degradation. This process takes place with a lower Li diffusion barrier compared to bulk Si. The improved kinetics and the absence of volume expansion settle silicene as a potential anode for LIB. <sup>[140]</sup> An extended study of this topic will be presented in the next chapters.

In the practice the layers of Silicene can be stabilized through terminations of hydrogen or hydroxide, forming the polysilane (Si<sub>6</sub>H<sub>6</sub> the analogue of graphane) and siloxene (Si<sub>6</sub>H<sub>3</sub>OH<sub>3</sub>)<sup>1</sup>. These phases were synthesized for the first time by Wöhler in 1863 <sup>[141]</sup> who studied the effects of acid in CaSi<sub>2</sub> (**Equation 2**). This last one has planes composed of Si<sub>6</sub> honeycomb rings with Ca intercalated in between, and by an acid treatment at low temperatures a yellow-green powder was obtained. <sup>[142]</sup> Subsequently, in 1921 Kautsky <sup>[143]</sup> modified the synthesis and obtained a gray-green compound called “Siloxene”. From the experimental data he suggested a structure constituted of planes of Si<sub>6</sub> honeycomb rings connected by oxygen bridges with each Si bonded to a hydrogen above or below the plane. Since the oxygen insertion in the Si planes causes stress and eventually structure degradation, no crystallinity evidence was found.



It was only until 1979 when Weiss *et al* <sup>[144,145]</sup> synthesized a crystalline Wöhler siloxene and performed the first structural characterizations. They proposed a structure of Si planes terminated by H or OH and no O inserted into the Si-Si bond system. They claimed that in the presence of moisture, the siloxene undergoes hydrolysis of Si-H to Si-OH followed by a condensation to Si-O-Si. These results were later confirmed by a powder and single crystal XRD characterization by Weber *et al* <sup>[146]</sup>. Posteriorly, Dahn *et al* <sup>[147,148]</sup> attributed presence of Si-O-Si

---

<sup>1</sup> Note that the terms silicene, siloxene, siloxane and polysilane are often misled in the literature; silicene refers to the monoatomic single layer of Si<sub>6</sub> honeycomb rings, siloxene to the bulk OH, H terminated silicene, siloxane to compounds made essentially from Si-O-Si bonds and polysilane to the H terminated silicene.

groups to the siloxene oxidation into a glassy SiO<sub>2</sub> by exposure to air and moisture, this crosslinking is intensified by thermal annealing >300°C leading to decomposition into SiO<sub>2</sub>. Finally, Yamanaka *et al* <sup>[149]</sup> synthesized layered polysilane (Si<sub>6</sub>H<sub>6</sub>) by topotactic reaction of CaSi<sub>2</sub> at -30°C with no hydrogen evolution, reactions carried out at higher temperatures resulted in oxidized siloxenes. The polysilane has a considerable amount of highly reactive dangling bonds, thus it is extremely reactive and complicated to handle. <sup>[125]</sup> Since the siloxene synthesis is different from conventional bulk Si, for a long time its research and understanding have remained in the organosilicon domain, being considered as a silicon-based polymer. This assumption was reinforced by the fact that oxygen serves as a link between two silicon atoms, allowing polymerization of Si-clusters to macroscopic structures. <sup>[150]</sup> As a matter of fact, this Si-O bonding originates three modifications for the siloxene structure (**Figure 16**); i) the Wöhler siloxene, a quasi-two-dimensional structure similar to the bulk c-Si (111) planes, except that each Si atom is bonded to other three Si and one OH or H. This structure can lower its energy by oxygen insertion in the planes to form ii) the Kautsky siloxene, in which the Si<sub>6</sub> rings are interconnected by oxygen bridges and iii) isolated Si chains connected via Si-O-Si. <sup>[150]</sup>

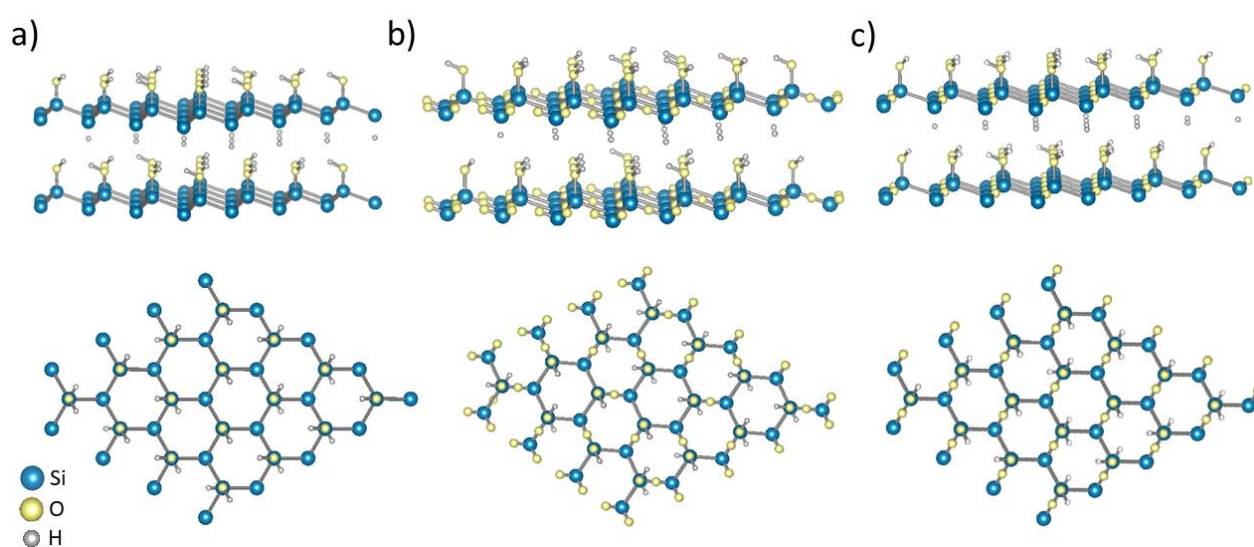


**Figure 16.** Structural model of the different siloxene modifications. a) corrugated silicon layers with three Si-Si bonds and alternating -H or -OH substituents (Wöhler siloxene). b) two-dimensional Si sheets made of Si<sub>6</sub> rings linked by oxygen bridges (Kautsky siloxene). c) one dimensional Si-Si chain interconnected by Si-O bonds.

Diverse modifications have been performed on the siloxene and polysilane, here, the synthesis conditions play an important role in the specific reaction products. <sup>[125]</sup> The following segment presents a brief revision of these particular synthesis. (**Figure 17**)

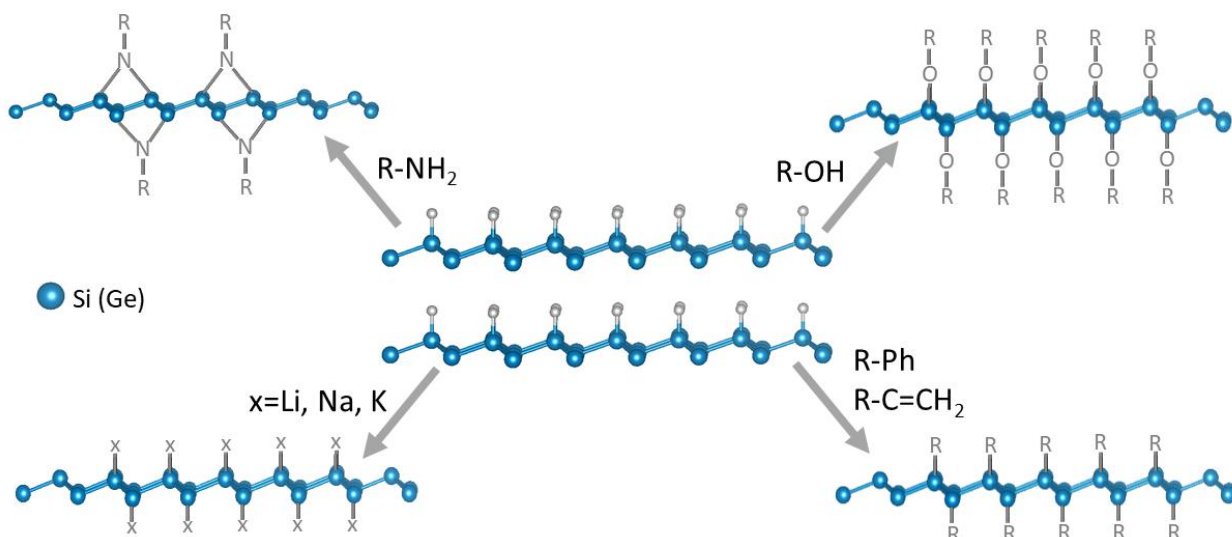


**Figure 17.** Synthetic routes for the preparation of organic modified siloxene (Germanane).

*Organic modification.* As observed in the figure, it is possible to introduce/intercalate different organic groups in the siloxene and polysilane layers. For example, unsaturated organic groups like alkenes and alkynes assisted by a catalyzer. These organic moieties do not only intercalate but also react with Si to form Si-C linkages, originating the characteristic IR vibrations of organic molecules (Si-CH<sub>2</sub> and CH) and a decrease in the Si-H signal intensity, indicators of a covalent attachment with the silicon. In the process the original siloxene/polysilane backbone is oxidized. <sup>[129,132,142]</sup>

The Si-C bond can be inserted as well via the Grignard reagent (PhMgBr). This method allows the synthesis of phenyl-modified and oxygen-free silicon nanosheets that are more stable towards oxidation and hydrolysis. The presence of Si-Ph bonds is determined through IR and <sup>1</sup>H NMR by the identification of the aromatic C=C bond and the different hydrogen environments of the phenyl group, respectively. The introduction of organic aromatic groups broadens the light absorption ranges and has applications in photovoltaics <sup>[129,132,142,151]</sup>. Finally,

the use of a HCl solution in methanol, butanol, C<sub>12</sub>H<sub>25</sub>, Benzyl alcohol or CH<sub>2</sub>COOMe forms the corresponding alkoxide-terminated organosiloxenes (Si<sub>6</sub>H<sub>5</sub>OR, where R= methanol, ethanol, butanol, C<sub>12</sub>H<sub>25</sub>, benzyl alcohol or CH<sub>2</sub>COOMe).<sup>[132,142]</sup> This process allows as well the production of carbon coated sheets by a non-oxidative pyrolysis, a better dispersion in organic solvents by the introduction of Si-C or Si-N bonds and a tuning of the band gap depending on the interlayer distance.<sup>[137]</sup> While c-Si has an indirect band gap and shows extremely weak luminescence, the Si sheets and chain polymer have a direct band gap resulting in a strong visible and near-UV photoluminescence.<sup>[152]</sup>

*Amination.* The Si center experiences a facile nucleophilic attack by N due to the Si<sup>δ+</sup>-H<sup>δ-</sup> polarization. This way by reacting Siloxene or polysilane with N-Decylamine or N-Butylamine the amine group is inserted on the surface. The Si-H bonds are transformed into Si-NR, subsequently by reaction with another Si-H into Si-NR-Si, originating a mixed composition of Si-NH-R and Si-NR-Si bonds. The IR confirmed the presence of the Si-N-Si vibrations and the absence of Si-H, N-H, Si-O ones. The obtained nanosheets are oxygen-free.<sup>[129,142]</sup>

*Exfoliation.* Several methods can be employed to achieve the exfoliation of the siloxene and polysilane layers. One of them is the Mg doping of CaSi<sub>2</sub>. This action weakens the electrostatic interaction between Ca<sup>2+</sup> and the [Si<sub>n</sub>] layers, by reducing the Si charge, producing CaSi<sub>1.85</sub>Mg<sub>0.15</sub>. The Ca is deintercalated with polyamine hydrochloride (PAHCl) to obtain nanosheets. The exfoliation occurred preferentially in the sections where Mg atoms were present and the obtained nanosheets are oxidized.<sup>[129,142,153]</sup> Also, the CaSi<sub>2</sub> can be doped with K, the produced silicon nanosheets have lower degree of oxidation and a high degree of ordering.<sup>[129]</sup>

Another method for exfoliation is the dispersion of siloxene/polysilane in a solution of sodium dodecyl sulfate (SDS) surfactant. Silicon nanosheets with lateral dimensions of <200 nm are obtained after several days of reaction. In this case the cleavage occurred thorough the

particle rather than on a layer by layer basis starting from the surface. The electron diffraction showed the presence of crystalline Siloxene, although the eventual oxidation of the layers cannot be prevented. <sup>[142,154]</sup>

In addition, silicon nanoflakes can be prepared via a solid state reaction, by heating a mixture of  $\text{CaSi}_2$  and  $\text{NiCl}_2$  at  $350^\circ\text{C}$  under Ar atmosphere to obtain the silicon nanoflakes and a mixture of  $\text{CaCl}_2$  and  $\text{NiSi}_2$ . The  $\text{CaCl}_2$  is easily removed with dimethylformamide (DMF), but the  $\text{NiSi}_2$  remains. If the reaction is performed with  $\text{TaCl}_5$ , the  $\text{TaCl}_n$  and  $\text{CaCl}_2$  by-products are removed by washing with ethanol. The resulting silicon nanoflakes are in agreement with Kautsky siloxene, the sheets are bridged by Ca atoms providing additional structural stability. <sup>[131,132,155]</sup> Lastly, the interlayer distance can be controlled until complete exfoliation by the intercalation of organic functional groups of different sizes, the bulkier the group the larger the interlayer distance and the weaker the interlayer adhesion. The complete exfoliation is assisted by sonication, this step determines the size and quality of the nanosheets. <sup>[129,137]</sup>

#### Germanene/Germanane

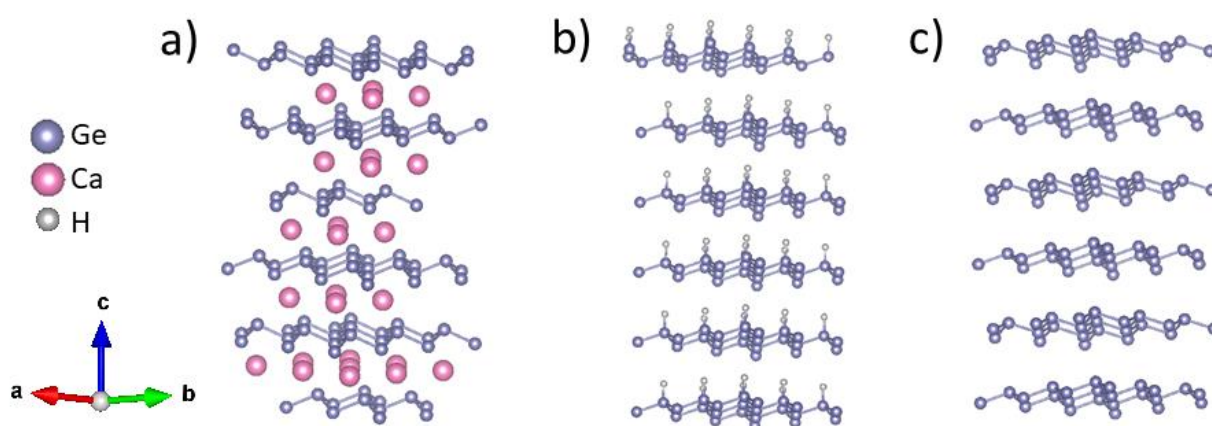


**Figure 18.** Structural model of a)  $\text{CaGe}_2$ , b) Germanane ( $\text{GeH}_n$ ) and c) Germanene.

The prediction and successful synthesis of silicene and siloxene opened the quest to find the graphene germanium analogue, the germanene. This material, similarly to silicene, consists of



a buckled Ge honeycombs monolayer, its free-standing form does not exist in nature. Although, it has been successfully deposited on metallic substrates like Au(111), Ag(111), Cu(111) by molecular beam epitaxy in ultra-high vacuum. <sup>[156]</sup> The choice of substrate is crucial as interactions with the deposited Ge atoms can take place, eg. in Ag (111) Ge atoms prefer to stabilize in Ag<sub>2</sub>Ge, <sup>[157]</sup> and the degree of buckling can be influenced. Then, a substrate that interacts weakly with germanene must be used to obtain free-standing monolayers. <sup>[132,134–136]</sup>

Due to its 2D nature the germanene has electron mobility 5 times higher than bulk Ge and the ability to undergo topological functionalization that produces a series of electronic states like semi-metallic, semiconducting, superconducting and trivial insulating. Applications include low-energy electronics, piezo-magnetism and thermoelectricity. Its band gap can be tuned by applying an electric field perpendicular direction to the sheets, property of great interest for transistor applications. A monolayer of hydrogen terminated germanene has already been used as a transistor. <sup>[138]</sup> Unfortunately, most of these properties are hindered by its instability at ambient conditions. <sup>[133]</sup>

The functionalization of germanene is an effective strategy to tailor physical and chemical properties (band gap, thermal stability, etc.), depending on the nature of the ligand. Functionalization includes fluorination, hydrogenation, organic group termination, foreign element doping. <sup>[156]</sup>

*Fluorination.* The F diffusion in the CaGe<sub>2</sub> lattice segregates the crystals into Ge and CaF<sub>2</sub> while maintaining their layered structure. With this technique depending on the F concentration monolayer, bilayer and trilayer germanene are stabilized. <sup>[158]</sup>

*Hydrogenation.* The hydrogenation to form the germanane (analogue of graphane) with a puckered structure (like siloxene) with a mix sp<sup>2</sup>-sp<sup>3</sup> hybridization was first reported in 2000. <sup>[156,159]</sup> Similarly to CaSi<sub>2</sub>, CaGe<sub>2</sub> undergoes a topotactic deintercalation of Ca at -30°C in concentrated HCl to form the germanane. **(Equation 3)** <sup>[133]</sup> The formation of germanane is

accompanied by a change in color from the gray-metallic in  $\text{CaGe}_2$  to red in germanane. <sup>[159]</sup> As observed for siloxene, the germanane stabilizes in the polymorphs that are inherent to the parent  $\text{CaGe}_2$  compound, the tr-6 (R-3m) trigonal-rhombohedral with a 6-fold stacking sequence and the 2H structure (P6<sub>3</sub>mc) hexagonal structure with 2-fold stacking sequence. <sup>[160]</sup>



Contrary to siloxene, the formation of germanane does not lead to a hydrolysis reactions even at temperatures  $>0^\circ\text{C}$ . <sup>[125]</sup> Therefore, the product is a hydrogen-terminated Ge honeycomb layers (isomorphic to (111) bulk Ge) linked by van der Waals forces, which are stable in air (in contrast to polysilane ( $\text{Si}_6\text{H}_6$ )). The absence of hydrolysis is an indicator of the different oxidation behavior of Si and Ge sheets, the binding energy of the Si-O bonds (8.0 eV) is stronger than Ge-O (6.6 eV) and the Si-H (3.0 eV) is slightly weaker than Ge-H (3.2 eV). The absence of  $-\text{OH}$  bonds shifts the photoluminescence energies to lower values compared to siloxene. <sup>[152]</sup> Other way, prolonged moisture exposure of germanane eventually leads to the formation of Ge-OH bonds, forming the Germoxene  $\text{Ge}_6\text{OH}_3\text{H}_3$ . <sup>[125,161]</sup> Germanane has been reported to be stable up to  $75^\circ\text{C}$  above which amorphization and dehydrogenation occur. <sup>[162]</sup>

The germanane layers can be exfoliated into nanosheets (GeNS), by mechanical processes, like scotch tape or sonication. <sup>[162,163]</sup> These GeNS have buckled honeycomb structures identical to Ge (111) but are easily oxidized. This issue can be addressed by the introduction of covalent bonds improving the chemical and thermal stability. <sup>[164]</sup>

*Organic group termination.* The formation of  $(\text{GeCH}_3)_n$  (methyl terminated germanane) has been reported by reacting  $\text{CaGe}_2$  with  $\text{CH}_3\text{I}/\text{H}_2\text{O}$ . The prepared  $\text{GeCH}_3$  had more  $-\text{H}$  than  $-\text{CH}_3$  terminations and oxidized germanane ( $\text{GeO}_x$ ). The crystals obtained by this method ( $\approx 1\text{mm}$  and  $<100\ \mu\text{m}$  thick) share the same honeycomb lattice as in  $\text{CaGe}_2$  and the thermal stability is increased to  $250^\circ\text{C}$  ( $\text{GeH} = 150^\circ\text{C}$ ). <sup>[165]</sup> A non-oxidative synthesis route that produces homogeneously covered  $\text{GeCH}_3$  to avoid local variations in the electronic structure, can be

performed by limiting the hydrogen source (water) and using  $\text{CH}_3\text{I}$  in  $\text{CH}_3\text{N}$ . This  $\text{GeCH}_3$  has an increased ratio  $-\text{CH}_3/-\text{H}$  with no oxidation, it is air stable and has a greater thermal stability ( $380^\circ\text{C}$ ).<sup>[166]</sup>

This organic modification can be extended to other functional groups; by reacting  $\text{CaGe}_2$  with  $-\text{CH}_2\text{OCH}_3$ ,  $-\text{CH}_2\text{CH}=\text{CH}_2$ ,  $-\text{CH}_3$ ,  $-\text{CH}_2\text{CH}_3$ ,  $\text{CH}_3\text{I}/\text{CH}_3\text{CN}$ , etc., in  $\text{HCl}$  resulting in  $\text{Ge}_x\text{H}_{1-x}$ .<sup>[167]</sup> The ligand size and electron withdrawing/donating properties have a strong influence on the final product; smaller ligands show almost full replacement of  $\text{Ge-H}$  bonds by  $\text{Ge-R}$  while bigger ones lead to partial hydrogenation of the framework. The band gaps and the Raman shifts are dictated by the relative  $\text{Ge-H}/\text{Ge-R}$  ratio in a similar fashion to the Vegard's Law. Larger and more electronegative ligands expand the germanane framework and lower the energy of the  $\text{Ge-R}$  interactions, reducing the band gap.<sup>[167,168]</sup> The methyl terminated germanane shows as well enhanced visible-light driven photocatalytic properties.<sup>[168]</sup>

*Foreign element doping.* The introduction of foreign elements in the germanane structure is done by doping the  $\text{CaGe}_2$  precursor with group 13, 14 or 15 elements that remain in the backbone after topotactic deintercalation. For instance,  $\text{Ge}$  can be partially substituted by  $\text{As}$  (1.1%),  $\text{Ga}$  (2.3%)<sup>[169]</sup>,  $\text{P}$ <sup>[170]</sup> and  $\text{Sn}$ . The  $\text{Ge}_{0.91}\text{Sn}_{0.09}\text{H}_{0.91}(\text{OH})_{0.091}$ <sup>[171]</sup> and  $\text{Si}_{1-x}\text{Ge}_x\text{H}_{1-y}(\text{OH})_y$ <sup>[125]</sup> alloys have been reported, the dopant content is determined by the maximum quantity of  $\text{Sn}$  ( $\text{Si}$ ) that can be incorporated in the precursor Zintl phase  $\text{Ca}(\text{Ge}_{1-x}\text{Sn}_x)_2$ ,  $\text{Ca}(\text{Si}_{1-x}\text{Ge}_x)_2$ .<sup>[171]</sup> In both cases the  $\text{Ge}$  is terminated with  $\text{H}$  while the  $\text{Sn}$  ( $\text{Si}$ ) with  $\text{OH}$ . Unfortunately these phases decompose rapidly at ambient conditions.<sup>[125,169,171]</sup>

*Alkali adsorption/intercalation.* The adsorption of more than one  $\text{Li}$  in germanene is favored in both sides of the layer. Calculations predict the adsorption of a total of 8  $\text{Li}$  atoms, 4 above and 4 below a single plane, with a good electron mobility and a  $\text{Li}$  diffusion barrier between 0.21-0.76 eV which is lower than silicene (1.2 eV). Based on a single and bilayer germanene the theoretical capacity are 369 and 276  $\text{mAh/g}$ , respectively.<sup>[172]</sup> The adsorption of  $\text{Na}$  has been

theoretically predicted as well in germanene and germanane. <sup>[173]</sup> The exfoliated germanane has been used as anode in LIB, with a reversible capacity of 1108 mAh/g. The advantage of the use of a 2D material in batteries is that the bulk diffusion can be eliminated, improving the rate capability. <sup>[163]</sup>

## 5 Conclusion and perspectives

This review provided a comprehensive study of the use of silicon and germanium for battery applications. The electrochemical mechanism for lithiation is highlighted based on a combination of different characterization techniques, while the sodiation and potassiation is studied based on the limited available information. For the lithiation the crystalline silicon and germanium transform into a series of amorphous lithiated intermediates and only a crystalline phase is observed at the end of the discharge, corresponding to  $\text{Li}_{15}\text{Si}_4$ . Upon delithiation the system is not able to recover the crystalline network and an amorphous Si and Ge are obtained. By comparing all the reports in the literature one can notice slight differences, indeed the cycling conditions such as particle size, C/rate, electrode formulation and morphology might impact the formed intermediates and cyclability. These phenomena are particularly noticeable for Ge. For the sodiation and potassiation of both Si and Ge, it is believed that their crystalline phase does not react whereas the amorphous one does, highlighting the role of the morphology and structure. It is known that the alloying reaction between Si /Ge and an alkali ion is accompanied by a series of challenges, including a volume expansion that can attain values as high as 300%, particle pulverization and a continuous expose of new surface to the electrolyte causing an uncontrolled and excessive growth of the SEI layer. All these factors will eventually affect the cycle life of the electrode. In order to address these challenges several strategies have been proposed, for instance the use of nanostructures specifically designed to host the volume expansion while maintaining a good structural stability and a better conductive network. Others may include the use of an

adequate binder to ensure the integral stability of the electrode and its adherence to the current collector; or the use of an effective electrolyte formulation that will promote the formation of a good SEI layer preventing further electrolyte decomposition. In such way, the structure and morphology are very important to ensure a good cyclability, motive for this review to cover as well a new family of layered Si/Ge-based compounds, the so-called Zintl phases. These compounds have been known for a long time, their high versatility allows an easy tuning of their properties for specific applications, and only until recently have been used in batteries. In fact a layered compound is beneficial for buffering the volume expansion and improving the electronic conductivity, enabling high power applications. Undoubtedly, representing a great interest, not only for LIB but also for post-LIB (NIB, KIB). Several theoretical studies foresee excellent cyclability for various battery systems, while the experimental reports remain limited for the moment. Therefore, the quest is opened for the study of these new Zintl phases, including their modification, their electrochemical mechanism and different intermediates involved. The aforementioned is necessary to successfully address the different challenges from a fundamental perspective, allowing to extract the best performance of each electrode material. This step is crucial for the implementation of Si and Ge-based anodes at the industrial level.

- [1] M. Winter, B. Barnett, K. Xu, *Chem. Rev.* **2018**, *118*, 11433.
- [2] K. Kubota, S. Komaba, *J. Electrochem. Soc.* **2015**, *162*, A2538.
- [3] N. Yabuuchi, K. Kubota, M. Dahbi, S. Komaba, *Chem. Rev.* **2014**, *114*, 11636.
- [4] G. Xu, R. Amine, A. Abouimrane, H. Che, M. Dahbi, Z. Ma, I. Saadoune, J. Alami, W. L. Mattis, F. Pan, Z. Chen, K. Amine, *Adv. Energy Mater.* **2018**, *1702403*, 1.
- [5] I. Sultana, M. M. Rahman, Y. Chen, A. M. Glushenkov, *Adv. Funct. Mater.* **2018**, *28*, 1.
- [6] K. Kubota, M. Dahbi, T. Hosaka, S. Kumakura, S. Komaba, *Chem. Rec.* **2018**, *18*, 459.
- [7] S. Mukherjee, Z. Ren, G. Singh, *Nano-Micro Lett.* **2018**, *10*, 70.
- [8] S. Y. Hong, Y. Kim, Y. Park, A. Choi, N.-S. Choi, K. T. Lee, *Energy Environ. Sci.* **2013**, *6*, 2067.
- [9] C. Nithya, S. Gopukumar, *Wiley Interdiscip. Rev. Energy Environ.* **2015**, *4*, 253.
- [10] Y. Jin, B. Zhu, Z. Lu, N. Liu, J. Zhu, *Adv. Energy Mater.* **2017**, *1700715*, In press.

- [11] K. Feng, M. Li, W. Liu, A. G. Kashkooli, X. Xiao, M. Cai, Z. Chen, *Small* **2018**, *14*.
- [12] Y. Han, ning Lin, T. Xu, T. Li, J. Tian, Y. Zhu, Y. Qian, *Nanoscale* **2018**.
- [13] C. H. Lim, T. Y. Huang, P. S. Shao, J. H. Chien, Y. T. Weng, H. F. Huang, B. J. Hwang, N. L. Wu, *Electrochim. Acta* **2016**.
- [14] L. Zhang, X. Hu, C. Chen, H. Guo, X. Liu, G. Xu, H. Zhong, S. Cheng, P. Wu, J. Meng, Y. Huang, S. Dou, H. Liu, *Adv. Mater.* **2016**.
- [15] Y. Xu, E. Swaans, S. Basak, H. W. Zandbergen, D. M. Borsa, F. M. Mulder, *Adv. Energy Mater.* **2016**, *6*, 1.
- [16] J. Sangster, A. D. Pelton, *Phase Diag. Eval. Sect. II* **1992**, *13*, 67.
- [17] M. K. Jangid, A. S. Lakhnot, A. Vemulapally, F. J. Sonia, S. Sinha, R. O. Dusane, A. Mukhopadhyay, *J. Mater. Chem. A* **2018**, *6*, 3422.
- [18] H. Jung, P. K. Allan, Y. Y. Hu, O. J. Borkiewicz, X. L. Wang, W. Q. Han, L. S. Du, C. J. Pickard, P. J. Chupas, K. W. Chapman, A. J. Morris, C. P. Grey, *Chem. Mater.* **2015**, *27*, 1031.
- [19] T. Kennedy, M. Brandon, K. M. Ryan, *Adv. Mater.* **2016**.
- [20] Q. Yang, Z. Wang, W. Xi, G. He, *Electrochem. commun.* **2019**, *101*, 68.
- [21] S. D. Beattie, D. Larcher, M. Morcrette, B. Simon, J.-M. Tarascon, *J. Electrochem. Soc.* **2008**, *155*, A158.
- [22] S. Lee, S. Chul, Y. Han, *J. Power Sources* **2019**, *415*, 119.
- [23] X. Lu, E. R. Adkins, Y. He, L. Zhong, L. Luo, S. X. Mao, C. M. Wang, B. A. Korgel, *Chem. Mater.* **2016**.
- [24] M. N. Obrovac, V. L. Chevrier, *Chem. Rev.* **2014**, *114*, 11444.
- [25] J. Li, J. R. Dahn, *J. Electrochem. Soc.* **2007**, *154*, A156.
- [26] F. Wang, L. Wu, B. Key, X. Yang, C. P. Grey, Y. Zhu, J. Graetz, *Adv. Energy Mater.* **2013**, *3*, 1324.
- [27] M. N. Obrovac, L. J. Krause, *J. Electrochem. Soc.* **2007**, *154*, A103.
- [28] J. Graetz, C. C. Ahn, R. Yazami, B. Fultz, *J. Electrochem. Soc.* **2004**, *151*, A698.
- [29] A. Kohandehghan, K. Cui, M. Kupsta, J. Ding, E. M. Lotfabad, W. P. Kalisvaart, D. Mitlin, E. Memarzadeh Lotfabad, W. P. Kalisvaart, D. Mitlin, *Nano Lett.* **2014**, *14*, 5873.
- [30] L. Baggetto, P. H. L. Notten, *J. Electrochem. Soc.* **2009**, *156*, A169.
- [31] M. Gu, Y. He, J. Zheng, C. Wang, *Nano Energy* **2015**, *17*, 366.
- [32] X. H. Liu, Y. Liu, A. Kushima, S. Zhang, T. Zhu, J. Li, J. Y. Huang, *Adv. Energy Mater.* **2012**, *2*, 722.
- [33] M. N. Obrovac, L. Christensen, *J. Electrochem. Soc.* **2004**, *7*, A93.
- [34] B. Key, M. Morcrette, J.-M. Tarascon, C. P. Grey, *J. Am. Chem. Soc.* **2011**, *133*.
- [35] V. L. Chevrier, L. Liu, D. B. Le, J. Lund, B. Molla, K. Reimer, L. J. Krause, L. D. Jensen, E. Figgemeier, K. W. Eberman, *J. Electrochem. Soc.* **2014**, *161*, A783.

- [36] V. L. Chevrier, J. R. Dahn, **2009**, 454.
- [37] D. S. M. Iaboni, M. N. Obrovac, *J. Electrochem. Soc.* **2016**, *163*, A255.
- [38] M. Ashuri, Q. He, L. L. Shaw, *Nanoscale* **2016**, *8*, 74.
- [39] S. W. Lee, I. Ryu, W. D. Nix, Y. Cui, *Extrem. Mech. Lett.* **2015**, *2*, 15.
- [40] K. C. Klavetter, S. M. Wood, Y. M. Lin, J. L. Snider, N. C. Davy, A. M. Chockla, D. K. Romanovicz, B. A. Korgel, J. W. Lee, A. Heller, C. B. Mullins, *J. Power Sources* **2013**, *238*, 123.
- [41] H. Jung, P. K. Allan, Y. Y. Hu, O. J. Borkiewicz, X. L. Wang, W. Q. Han, L. S. Du, C. J. Pickard, P. J. Chupas, K. W. Chapman, A. J. Morris, C. P. Grey, *Chem. Mater.* **2015**.
- [42] J. N. Weker, N. Liu, S. Misra, J. C. Andrews, Y. Cui, M. F. Toney, *Energy Environ. Sci.* **2014**, *7*, 2771.
- [43] W. Tang, Y. Liu, C. Peng, M. Y. Hu, X. Deng, M. Lin, J. Z. Hu, K. P. Loh, *J. Am. Chem. Soc.* **2015**, *137*, 2600.
- [44] L. C. Loaiza, N. Louvain, B. Fraisse, A. Boulaoued, A. Iadecola, P. Johansson, L. Stievano, V. Seznec, L. Monconduit, *J. Phys. Chem. C* **2018**, *122*, 3709.
- [45] L. Y. Lim, S. Fan, H. H. Hng, M. F. Toney, *Adv. Energy Mater.* **2015**, *5*.
- [46] H. Axel, H. Schafer, A. Weiss, *Z. Naturforschg* **1966**, 115.
- [47] R. Nesper, H. G. von Schnering, *J. Solid State Chem.* **1987**, *70*, 48.
- [48] T. D. Hatchard, J. R. Dahn, *J. Electrochem. Soc.* **2004**, *151*, A838.
- [49] M. Zeilinger, D. Benson, U. Häussermann, T. F. Fässler, *Chem. Mater.* **2013**, *25*, 1960.
- [50] J. Y. Kwon, J. Heon, S. M. Oh, *Electrochim. Acta* **2010**, *55*, 8051.
- [51] M. Zeilinger, V. Baran, L. Van Wüllen, U. Haussermann, T. F. Fässler, *Chem. Mater.* **2013**, *25*, 4113.
- [52] M. Gu, Z. Wang, J. G. Connell, D. E. Perea, L. J. Lauhon, F. Gao, C. Wang, *ACS Nano* **2013**, *7*, 6303.
- [53] M. Tang, V. Sarou-Kanian, P. Melin, J.-B. Leriche, M. Ménétrier, J.-M. Tarascon, M. Deschamps, E. Salager, *Nat. Commun.* **2016**, *7*, 13284.
- [54] N. M. Trease, T. K.-J. Köster, C. P. Grey, *Electrochem. Soc. Interface-Fall 2011* **2011**, *20*, 69.
- [55] A. J. Morris, C. P. Grey, C. J. Pickard, *Phys. Rev. B* **2014**, *90*, 54111.
- [56] A. S. Cattaneo, S. Dupke, A. Schmitz, J. P. Badillo, M. Winter, H. Wiggers, H. Eckert, *Solid State Ionics* **2013**, *249–250*, 41.
- [57] B. Key, R. Bhattacharyya, M. Morcrette, V. Seznec, J. M. Tarascon, C. P. Grey, *J. Am. Chem. Soc.* **2009**, *131*, 9239.
- [58] K. Ogata, E. Salager, C. J. Kerr, A. E. Fraser, C. Ducati, A. J. Morris, S. Hofmann, C. P. Grey, *Nat. Commun.* **2014**, *5*, 3217.
- [59] M. K. Y. Chan, C. Wolverton, J. P. Greeley, P. Greeley, *J. Am. Chem. Soc.* **2012**, *134*, 1.

- [60] L. Baggetto, E. J. M. Hensen, P. H. L. Notten, *Electrochim. Acta* **2010**, *55*, 7074.
- [61] L. Y. Lim, N. Liu, Y. Cui, M. F. Toney, *Chem. Mater.* **2014**.
- [62] L. Y. Lim, S. Fan, H. H. Hng, M. F. Toney, *J. Phys. Chem. C* **2015**, *119*, 22772.
- [63] S. Yoon, C.-M. Park, H.-J. Sohn, *Electrochem. Solid-State Lett.* **2008**, *11*, A42.
- [64] A. J. J. Morris, C. P. P. Grey, C. J. J. Pickard, *Phys. Rev. B - Condens. Matter Mater. Phys.* **2014**, *90*, 54111.
- [65] L. Y. Lim, S. Fan, H. H. Hng, M. F. Toney, *J. Phys. Chem.* **2015**, *119*, 22772.
- [66] S. Huang, L. Liu, Y. Zheng, Y. Wang, D. Kong, Y. Zhang, Y. Shi, L. Zhang, O. G. Schmidt, H. Y. Yang, *Adv. Mater.* **2018**, *1706637*, 1.
- [67] S. C. Jung, D. S. Jung, J. W. Choi, Y. K. Han, *J. Phys. Chem. Lett.* **2014**.
- [68] H. Wu, W. Liu, L. Zheng, D. Zhu, N. Du, C. Xiao, L. Su, L. Wang, *ChemistryOpen* **2019**, *8*, 298.
- [69] L. Baggetto, J. K. Keum, J. F. Browning, G. M. Veith, *Electrochem. commun.* **2013**, *34*, 41.
- [70] Q. Wang, C. Zhao, Y. Lu, Y. Li, Y. Zheng, Y. Qi, X. Rong, L. Jiang, X. Qi, Y. Shao, D. Pan, B. Li, Y.-S. Hu, L. Chen, *Small* **2017**, *1701835*, 1701835.
- [71] N. Lin, K. Shen, N. Lin, T. Xu, Y. Han, *R. Soc. Open Sci.* **2018**, *5*, 171477.
- [72] T. Kajita, T. Itoh, *Electrochim. Acta* **2016**, *195*, 192.
- [73] C. Y. Chou, G. S. Hwang, *Appl. Surf. Sci.* **2014**, *323*, 78.
- [74] F. Legrain, O. I. Malyi, S. Manzhos, *Solid State Ionics* **2013**.
- [75] W. Li, X. Sun, Y. Yu, *Small Methods* **2017**, *1*, 1600037.
- [76] A. Casimir, H. Zhang, O. Ogoke, J. C. Amine, J. Lu, G. Wu, Silicon-based anodes for lithium-ion batteries: Effectiveness of materials synthesis and electrode preparation. *Nano Energy* **2016**.
- [77] W. Liang, H. Yang, F. Fan, Y. Liu, X. H. Liu, J. Y. Huang, T. Zhu, S. Zhang, *ACS Nano* **2013**, *7*, 3427.
- [78] Y. Xu, M. Zhou, Y. Lei, *Adv. Energy Mater.* **2016**, *6*, 1.
- [79] L. Liu, J. Lyu, T. Li, T. Zhao, *Nanoscale* **2016**, *8*, 701.
- [80] X. Su, Q. Wu, J. Li, X. Xiao, A. Lott, W. Lu, B. W. Sheldon, J. Wu, *Adv. Energy Mater.* **2014**, *4*, 1.
- [81] F. Du, K. Wang, J. Chen, *J. Mater. Chem. A Mater. energy Sustain.* **2015**, *0*, 1.
- [82] D. Li, H. Wang, T. Zhou, W. Zhang, H. K. Liu, Z. Guo, *Adv. Energy Mater.* **2017**, *7*, 1.
- [83] M. N. Obrovac, V. L. Chevrier, *Chem. Rev.* **2014**, *114*, 11444.
- [84] J. K. Lee, K. B. Smith, C. M. Hayner, H. H. Kung, *Chem. Commun.* **2010**, *46*, 2025.
- [85] L. C. Loaiza, E. Salager, N. Louvain, A. Boulaoued, A. Iadecola, P. Johansson, L. Stievano, V. Seznec, L. Monconduit, *J. Mater. Chem. A* **2017**, *5*, 12462.
- [86] D. Dureau, B. Fraisse, F. Cunin, L. Monconduit, *Chem. Mater.* **2015**, *27*, 3226.



- [87] H.-J. Ahn, Y.-S. Kim, K.-W. Park, T.-Y. Seong, *Chem. Commun. (Camb)*. **2005**, 43.
- [88] M. K. Jangid, A. Vemulapally, F. J. Sonia, M. Aslam, *J. Electrochem. Soc.* **2017**, *164*, 2559.
- [89] Q. Zhao, Y. Huang, X. Hu, *Electrochem. commun.* **2016**, *70*, 8.
- [90] P. R. Abel, Y. M. Lin, T. De Souza, C. Y. Chou, A. Gupta, J. B. Goodenough, G. S. Hwang, A. Heller, C. B. Mullins, *J. Phys. Chem. C* **2013**, *117*, 18885.
- [91] Y. Kim, K. H. Ha, S. M. Oh, K. T. Lee, *Chem. - A Eur. J.* **2014**, *20*, 11980.
- [92] M. Li, Z. Wang, J. Fu, K. Ma, E. Detsi, *Scr. Mater.* **2019**, *164*, 52.
- [93] Z. Xu, J. Yang, H. Li, Y. Nuli, J. Wang, *J. Mater. Chem. A* **2019**, *7*, 9432.
- [94] A. M. Haregewoin, A. S. Wotango, B. J. Hwang, *Energy Environ. Sci.* **2016**, *9*, 1955.
- [95] L. Wang, J. Światowska, S. Dai, M. Cao, Z. Zhong, Y. Shen, M. Wang, *Mater. Today Energy* **2019**, *11*, 46.
- [96] A. Darwiche, L. Bodenes, L. Madec, L. Monconduit, H. Martinez, *Electrochim. Acta* **2016**.
- [97] L. Bodenes, A. Darwiche, L. Monconduit, H. Martinez, *J. Power Sources* **2015**, *273*, 14.
- [98] S. S. Komaba, M. Dahbi, N. Yabuuchi, K. Kubota, K. Tokiwa, S. Komaba, *Phys. Chem. Chem. Phys. Phys. Chem. Chem. Phys* **2014**, *16*, 15007.
- [99] L. Madec, V. Gabaudan, G. Gachot, L. Stievano, L. Monconduit, H. Martinez, *ACS Appl. Mater. Interfaces* **2018**, acsami.8b08902.
- [100] B. Lestriez, S. Bahri, I. Sandu, L. Roué, D. Guyomard, *Electrochem. commun.* **2007**, *9*, 2801.
- [101] Z. Karkar, D. Guyomard, L. Roué, B. Lestriez, *Electrochim. Acta* **2017**, *258*, 453.
- [102] G. Liu, S. Xun, N. Vukmirovic, X. Song, P. Olalde-Velasco, H. Zheng, V. S. Battaglia, L. Wang, W. Yang, *Adv. Mater.* **2011**, *23*, 4679.
- [103] B. Koo, H. Kim, Y. Cho, K. T. Lee, N. S. Choi, J. Cho, *Angew. Chemie - Int. Ed.* **2012**.
- [104] R. Nesper, *Zeitschrift fur Anorg. und Allg. Chemie* **2014**, *640*, 2639.
- [105] T. F. Fassler, *Zintl Phases*; 1992.
- [106] S. C. Sevov, In *Intermetallic compounds: Principles and Practice*; Westbrook, J. H.; Fleischer, R. L., Eds.; John Wiley & Sons, Ltd, 2002; Vol. 3.
- [107] R. Nesper, *Prog. Solid St. Chem.* **1990**, *20*, 1.
- [108] E. Mooser, W. B. Pearson, *Phys. Rev.* **1956**, *101*, 1608.
- [109] J. D. Corbett, *Chem. Rev.* **1985**, *85*, 383.
- [110] J. D. Corbett, *Angew. Chemie - Int. Ed.* **2000**, *39*, 670.
- [111] W. Van der Lugt, *J. Phys. Condens. Matter* **1996**, *8*, 6115.
- [112] R. Nesper, *Silicon Chem. From Atom to Ext. Syst.* **2007**, 171.
- [113] C. Belin, M. Tillard-charbonnel, *Prog. Solid State Chem.* **1993**, *22*, 59.
- [114] M. Q. Arguilla, *Electronic and Magnetic Materials from Two-dimensional Honeycomb Tin Lattices*, The Ohio State University, 2017.

- [115] A. Vegas, *Inorganic 3D structures*; Springer Berlin Heidelberg, 2011.
- [116] M. H. Zeilinger, *Synthesis, Characterization and Reactivity of Lithium-Containing Silicides, Germanides and Borosilicides*, TECHNISCHE UNIVERSITÄT MÜNCHEN, 2014.
- [117] V. L. Chevrier, J. W. Zwanziger, J. R. Dahn, *J. Alloys Compd.* **2010**, *496*, 25.
- [118] L. A. Stearns, J. Gryko, J. Diefenbacher, G. K. Ramachandran, P. F. McMillan, *J. Solid State Chem.* **2003**, *173*, 251.
- [119] B. Hans, G. Von Schnering, R. Nesper, J. Curda, *Angew. Chemie* **1980**, *1070*, 1033.
- [120] A. Kuhn, P. Sreeraj, R. Pöttgen, H. D. Wiemhöfer, M. Wilkening, P. Heitjans, *J. Am. Chem. Soc.* **2011**, *133*, 11018.
- [121] M. Zeilinger, T. F. Fässler, *Dalt. Trans.* **2014**, *43*, 14959.
- [122] G. R. Goward, N. J. Taylor, D. C. S. Souza, L. F. Nazar, *J. Alloy. Compd.* **2001**, *329*, 82.
- [123] X. Ma, F. Xu, T. M. Atkins, A. M. Goforth, D. Neiner, A. Navrotsky, S. M. Kauzlarich, *Dalt. Trans.* **2009**, 10250.
- [124] N. D. Cultrara, Y. Wang, M. Q. Arguilla, M. R. Scudder, S. Jiang, W. Windl, S. Bobev, J. E. Goldberger, *Chem. Mater.* **2018**, *30*, 1335.
- [125] M. S. Brandt, G. Vogg, M. Stutzmann, In *Silicon Chemistry: From the Atom to Extended Systems*; Jutzi, P.; Schubert, U., Eds.; Wiley-VCH Verlag GmbH & Co, 2007; pp. 194–213.
- [126] L. Zhao, D. J. Dvorak, M. N. Obrovac, *J. Power Sources* **2016**, *332*, 290.
- [127] M. Pelosi, M. Tillard, D. Zitoun, *J. Nanoparticle Res.* **2013**, *15*.
- [128] K. Annou, M. Pelosi, G. Gershinsky, F. Favier, Y. Cuminal, M. Tillard, D. Zitoun, *Mater. Renew. Sustain. Energy* **2014**, *3*.
- [129] M. A. Ali, M. R. Tchalala, *J. Phys. Conf. Ser.* **2014**, *491*, 12009.
- [130] H. Okamoto, Y. Sugiyama, H. Nakano, *Chem. - A Eur. J.* **2011**, *17*, 9864.
- [131] H. Itahara, H. Nakano, *Jpn. J. Appl. Phys.* **2017**, *56*, 05DA02.
- [132] M. J. S. Spencer, *Silicene: Structure, Properties and Applications*; 2016.
- [133] A. Molle, J. Goldberger, M. Houssa, Y. Xu, S. Zhang, *Nat. Publ. Gr.* **2017**.
- [134] C. Grazianetti, E. Cinquanta, A. Molle, *2D Mater.* **2016**, *3*.
- [135] S. Cahangirov, H. Sahin, G. Le Lay, A. Rubio, In *Introduction to the Physics of Silicene and other 2D Materials*; 2017; Vol. 930, pp. 13–40.
- [136] M. Houssa, A. Dimoulas, A. Molle, *J. Phys. Condens. Matter* **2015**, *27*, 253002.
- [137] A. Gupta, T. Sakthivel, S. Seal, *Prog. Mater. Sci.* **2015**, *73*, 44.
- [138] M. D'angelo, I. Matsuda, *Basics and Families of Monatomic Layers*; Elsevier Inc., 2019.
- [139] D. Jose, A. Datta, *Acc. Chem. Res.* **2014**, *47*, 593.
- [140] H. Oughaddou, H. Enriquez, M. R. Tchalala, H. Yildirim, A. J. Mayne, A. Bendounan, G. Dujardin, M. Ait Ali, A. Kara, *Prog. Surf. Sci.* **2015**, *90*, 46.
- [141] F. Wöhler, *Justus Liebigs Ann. Chem.* **1863**, *127*, 257.

- [142] H. Nakano, T. Ikuno, *Appl. Phys. Rev.* **2016**, *3*, 40803.
- [143] H. Kautsky, *Zeitschrift für Anorg. und Allg. Chemie* **1921**, *117*, 209.
- [144] A. Weiss, G. Beil, H. Meyer, *Z. Naturforsch., B* **1979**, *34b*, 25.
- [145] A. Weiss, G. Beil, H. Meyer, *Zeitschrift für Naturforsch.* **1979**, *34b*, 25.
- [146] U. Dettlaff-Weglikowska, W. Hönle, A. Molassioti-Dohms, S. Finkbeiner, J. Weber, *Phys. Rev. B* **1997**, *56*, 13132.
- [147] J. R. Dahn, B. M. Way, E. W. Fuller, W. J. Weydanz, J. S. Tse, D. D. Klug, T. Van Buuren, T. Tiedje, *J. Appl. Phys.* **1994**, *75*, 1946.
- [148] J. R. Dahn, B. M. Way, E. Fuller, *Phys. Rev. B* **1993**, *48*, 872.
- [149] K. Nishimura, Y. Nagao, S. Yamanaka, H. Matsu-Ura, *Japanese J. Appl. Physics, Part 2 Lett.* **1996**, *35*.
- [150] P. Deak, *Mod. Phys. Lett. B* **1993**, *7*, 1343.
- [151] Y. Sugiyama, H. Okamoto, T. Mitsuoka, T. Morikawa, K. Nakanishi, T. Ohta, H. Nakano, *J. Am. Chem. Soc.* **2010**, *132*, 5946.
- [152] L. J. P. Meyer, Z. Hajnal, T. Frauenheim, M. S. Brandt, G. Vogg, B. Szűcs, *Phys. Rev. B - Condens. Matter Mater. Phys.* **2001**, *64*, 1.
- [153] H. Nakano, T. Mitsuoka, M. Harada, K. Horibuchi, H. Nozaki, N. Takahashi, T. Nonaka, Y. Seno, H. Nakamura, *Angew. Chemie - Int. Ed.* **2006**, *45*, 6303.
- [154] H. Nakano, M. Ishii, H. Nakamura, *Chem. Commun. (Camb)*. **2005**, *2*, 2945.
- [155] H. Imagawa, H. Itahara, *Dalt. Trans.* **2017**, *46*, 3655.
- [156] N. Liu, G. Bo, Y. Liu, X. Xu, Y. Du, S. X. Dou, *Small* **2019**, 1805147.
- [157] M. E. Dávila, L. Xian, S. Cahangirov, A. Rubio, G. Le Lay, *New J. Phys.* **2014**, *16*.
- [158] R. Yaokawa, T. Ohsuna, Y. Hayasaka, H. Nakano, *ChemistrySelect* **2016**, *1*, 5579.
- [159] G. Vogg, M. S. Brandt, M. Stutzmann, *Adv. Mater.* **2000**, *12*, 1278.
- [160] X. Luo, E. Zurek, *J. Phys. Chem. C* **2015**, *120*, 793.
- [161] G. Vogg, L. J. P. Meyer, C. Miesner, M. S. Brandt, M. Stutzmann, *Monatshefte für Chemie* **2001**, *132*, 1125.
- [162] E. Bianco, S. Butler, S. Jiang, O. D. Restrepo, W. Windl, J. E. Goldberger, *ACS Nano* **2013**, *7*, 4414.
- [163] A. C. Serino, J. S. Ko, M. T. Yeung, J. J. Schwartz, C. B. Kang, S. H. Tolbert, R. B. Kaner, B. S. Dunn, P. S. Weiss, *ACS Nano* **2017**, *11*, 7995.
- [164] H. Yu, T. Helbich, L. M. Scherf, J. Chen, K. Cui, T. F. Fa, B. Rieger, J. G. C. Veinot, *Chem. Mater.* **2018**, *30*, 2274.
- [165] S. Jiang, S. Butler, E. Bianco, O. D. Restrepo, W. Windl, J. E. Goldberger, *Nat. Commun.* **2014**, *5*, 1.
- [166] S. Jiang, M. Q. Arguilla, N. D. Cultrara, J. E. Goldberger, *Chem. Mater.* **2016**, *28*, 4735.
- [167] S. Jiang, K. Krymowski, T. Asel, M. Q. Arguilla, N. D. Cultrara, E. Yanchenko, X. Yang, L. J.

- Brillson, W. Windl, J. E. Goldberger, *Chem. Mater.* **2016**, *28*, 8071.
- [168] Z. Liu, Z. Wang, Q. Sun, Y. Dai, B. Huang, *Appl. Surf. Sci.* **2019**, *467–468*, 881.
- [169] N. D. Cultrara, M. Q. Arguilla, S. Jiang, C. Sun, M. R. Scudder, R. D. Ross, J. E. Goldberger, *Beilstein J. Nanotechnol.* **2017**, *8*, 1642.
- [170] J. R. Young, B. Chitara, N. D. Cultrara, M. Q. Arguilla, S. Jiang, F. Fan, E. Johnston-Halperin, J. E. Goldberger, *J. Phys. Condens. Matter* **2015**, *28*.
- [171] M. Q. Arguilla, S. Jiang, B. Chitara, J. E. Goldberger, *Chem. Mater.* **2014**, *26*, 6941.
- [172] D. K. Sharma, S. Kumar, A. Laref, S. Auluck, *Comput. Condens. Matter* **2018**, *16*, e00314.
- [173] R. Bhuvaneshwari, V. Nagarajan, R. Chandiramouli, *Mater. Res. Express* **2019**, *6*, 35504.
- [174] S. Xu, X. Fan, J. Liu, Q. Jiang, W. Zheng, D. J. Singh, *Electrochim. Acta* **2019**, *297*, 497.
- [175] A. Y. Galashev, K. A. Ivanichkina, *J. Electrochem. Soc.* **2018**, *165*, A1788.
- [176] V. V. Kulish, O. I. Malyi, M.-F. Ng, Z. Chen, S. Manzhos, P. Wu, *Phys. Chem. Chem. Phys.* **2014**, *16*, 4260.